Manuscript acp-2020-294 – Author's replies to reviewers

*We thank gratefully the editor and two anonymous referees for careful reading and comments. Below are the referee's comments in **black**, and replies from the authors in **blue**. Please note that page and line numbers given below refer to the revised version of the manuscript* <u>*without*</u> *tracked-changes.*

<u>Anonymous Referee #1</u>

The paper presents an interesting comparison between the aerosol backscatter coefficients measured by two different lidar systems (a sophisticated multiwavelength lidar with elastic and Raman channels, and a ceilometer) and those obtained by a balloon-borne instrument performing in-situ measurements. The latter is taken as reference to validate the backscatter profiles provided by the lidars.
The paper is well written and describes a sound methodology that, besides providing the validation mentioned in the paper's title, can be useful for similar verifications at other sites.
I think the paper is worth publishing (although given its scope, focusing on techniques and methods rather than on atmospheric processes, perhaps the sister journal Atmospheric Measurement Techniques would provide a more suitable forum).
The authors may wish to consider the following remarks that in my view would improve the manuscript.

Main remarks

1. In the paper it is implied that the COBALD instrument is taken as the reference against which the lidar-derived backscatter coefficients are validated, on grounds that an in-situ instrument inherently provides "higher precision and signal-to-noise ratio compared to remote sensing measurements" (line 31, page 2). For this reason, I miss a more detailed description of the instrument specifications, namely, systematic (bias) and random (noise) error.

The accuracy and precision of COBALD BSR were estimated by Vernier et al. (2015) (Section 2.1) as 5 % and 1 %, respectively, at upper tropospheric conditions (which can be regarded as an upper limit here, due to the higher absolute signal measured in the lower troposphere). This previously missing information is now included in the manuscript (Page 5, Lines 7-8).

2. The above remark is somewhat linked to a seemingly lack of explanation for the mean deviations between the lidar-derived backscatter coefficients and those provided by the COBALD instruments in the PBL (+ 6% for RALMO and +13% for the ceilometer, below 2 km, (lines 23-24, page 1)). Is this just a random effect resulting from the limited dataset? Might negative differences be obtained for other datasets? Is this an effect resulting from the wavelength conversion and the FOV correction discussed respectively in sections 3.2 and 3.3? Does it come from other reasons (see next point).

Indeed, the uncertainties related with the wavelength conversion and the FOV correction, as well as spatial and temporal variability effects, contribute to the mean and standard deviations of our statistical comparison. A more detailed and quantitative discussion of the uncertainties associated with these effects is now included in the new Section 4.3.
In particular, concerning the wavelength conversion: "From Equation 1 we can derive that an error of 0.2 in AE, which is a conservative estimate considering the small difference between the wavelengths that are compared, results in an error of 5 % in β_{aer} for the 355-to-455 nm conversion, and 2.5 % for the 1064-to-940 nm conversion" (Page 15, Lines 9-11).
Concerning the FOV correction: "From Figure 2b, we can estimate an uncertainty of up to ± 20% in βaer for the PBL (for both 455 and 940 nm), due to variability of the correction factors in the range of AE = 0.8-1.5, which is not resolved by the parameterization of the FOV correction factors in AE-space." (Page 15, Lines 12-14).

Finally, about spatial and temporal variability: ”These effects can lead to large discrepancies over small altitude layers, as in the case of strong vertical gradients in βaer (e.g., top of boundary layer: Figure 4a-d), as well as potentially over larger altitude regions, due to the horizontal gradient of the βaer field around the station (e.g., in the case of the strongly outlying profiles of the statistical comparison: see Figures 5, 8). The lack of information on the aerosol size distribution and the high spatial and temporal variability of atmospheric aerosols prevent an accurate quantification of these artifacts, which inevitably affect the standard deviations of our statistical comparison" (Page 15, Lines 16-21).
Hence, we conclude: "Despite of these limitations, the comparison of individual profiles (Section 4.1) shows that both RALMO and CHM15K are able to achieve an excellent agreement with COBALD measurements, including the correct representation of fine and complex structures in the βaer vertical profiles (Figures 3-4, S2-S3). In particular, the case study of 12 July 2018 (Figures 4a-d) shows differences between the lidars and COBALD which are smaller than expected statistical uncertainty associated with the remote sensing measurements alone (10-15 %, see Section 2.1). This suggests that, under optimal conditions (such as, no wind shear, uniform βaer field, mono-modal aerosol size distribution), the deviations between the two lidars and COBALD are typically smaller than the average σ of our statistical comparison.” (Page 15, Lines 28 - Page 16, Line 1).

3. Related to the previous point, the authors put forward the possibility (lines 1-2 of page 13) that the 15% positive bias below 2.5 km (line 30 of page 12; by the way, shouldn’t it be rather 13%, cf. line 24 of page 1 and fig. 9f) be related to “minor unsolved geometric overlap issues in the ceilometer’s retrieval algorithm, or (more likely) related to the assumption of a constant lidar ratio (50 sr)”. Could this also be the cause for the (smaller (+6.5%)) positive bias in the RALMO vs. COBALD comparison below 2 km? The influence of an assumed lidar ratio could checked with relative ease. Have the authors done it?

The uncertainty associated with the assumption of a constant lidar ratio (50 sr) in the retrieval algorithm for CHM15K, which adds up to the uncertainties discussed in the previous comment, is now also discussed more in detail in Section 4.3.
"Using a similar ceilometer (Jenoptik CHM15kx), Wiegner and Geiss (2012) estimate that an error of ± 10 sr in lidar ratio leads to an error in βaer smaller than 2 % in the boundary layer. Ackermann (1998) shows that 50 ± 10 sr represents well the expected range of variability of the lidar ratio of continental aerosol in the infrared spectrum, for all RH conditions between 0-90 %. Therefore, this uncertainty conceivably plays a minor role compared to the effects discussed above.” (Page 15, Lines 24-27).
For RALMO, no a-priori assumption on lidar ratio is required for the backscatter retrieval (see Section 2.1). Therefore, this uncertainty only affects the CHM15K comparison. The sentence at Page 13, Lines 1-2 of the original manuscript was removed within the revision of the statistical comparison (see answer to comment 5 below).

4. It would also be advisable that the authors provide some indication on the statistical error in the measurements (estimated error bars), not only for the COBALD sondes, but also for the lidar-derived backscatter coefficients. That would help clarifying how much of the standard deviation found in the comparisons presented is due to the uncertainty of the measurements of each instrument, which must set a lower limit to that standard deviation affected as well, as the authors point out, by the differences between the atmosphere volumes measured by the sonde and by the lidars.

Information on the estimated mean statistical uncertainty of RALMO and CHM15K is now provided in Section 2.1. For RALMO “The mean statistical uncertainties associated with the retrieval of βaer at 355 nm from Raman inversion techniques are typically estimated as 15 % in the PBL (Pappalardo et al., 2004)." (Page 4, Lines 2-4). For CHM15K: “using a similar ceilometer (CHM15kx by Jenoptik, Germany), Wiegner and Geiss (2012) report a relative error of 10 % on βaer at 1064 nm retrieved by this method" (Page 4, Lines 14-15). The observed standard deviations of the statistical comparison, as well as the comparison of individual profiles, are now discussed in the context of these statistical uncertainties in Section 4.3 and Conclusions (see in particular Page 15 Line 30 - Page 16 Line 1, Page 17 Lines 4-7).

5. I would suggest restricting the use of relative differences in the comparisons of the backscatter coefficients to the layers with a medium to high aerosol content. I think using it in zones of low aerosol content or in the free troposphere is misleading, as small absolute differences will yield large figures when they are divided by a very small backscatter coefficient, which in turn is probably driven by statistical noise. In this respect, the authors should probably follow the criteria stated in section 4D of their reference Matthais et al., 2004. If the authors want to highlight something important coming out from these comparisons in terms of relative errors at those altitude ranges with little or no aerosol content, they should be more explicit.

Following this comment and one remark of Reviewer #2, the statistical comparison (including mainly Section 4 and Figures 5-10) has been strongly revised and improved. In particular, the following changes were made:

- Low and medium-high aerosol content measurements are separated according to an empirical threshold, and shown by different colors in Figures 5, 7, 8, 10.
- Mean and standard deviations profiles (Figures 5, 8) are calculated from medium-high aerosol content only, and the use of relative differences in the discussion is mainly restricted to medium-high aerosol content measurements.
- The probability density functions (Figures 6, 9) are calculated for medium-high aerosol content and all data separately.
- The Pearson correlation coefficient is now also calculated for medium-high aerosol content data, allowing to quantitatively evaluate the linearity of the correlation between the lidar and COBALD measurements.
- A new Section 3.3 (Page 9 Line 10 - Page 10 Line 17) was added to the manuscript, where we introduce the sorting of the data according to aerosol content, and formally define the compared quantities (Equations 3-6).

This approach allows to meaningfully quantify the deviations of medium-high aerosol content measurements at all altitudes, which is the main focus of this study, while at the same time not fully neglecting low aerosol content measurement at higher altitudes, which are important because a good agreement in the free troposphere ensures that all profiles are well calibrated (see Page 9, Lines 24-26).
We believe the revised statistical comparison is strongly improved compared to the previous version of the paper, both in terms of scientific content and clarity, and we thank the reviewer for this comment.

Minor issues

1. The statistical analyses of the comparisons of RALMO and the CHM15K ceilometer against COBALD are divided in figs. 6 and 9 in altitude zones, the first one being 0-2 km asl. However, in the text, when discussing the comparisons at the lowermost altitudes, the authors often use the 2.5 km limit (e.g. lines 25 and 28 in page 10, etc.). It would be easier for the reader to follow the discussions if the text and the figures would use the same limits.

Done. In the revised statistical comparison, we reduced the number of vertical intervals from three (0.8-2 km, 2-4 km, 4-6 km) to two (0.8-3 km, 3-6 km), and the limit value of z = 3 km is now used consistently throughout the manuscript.

2. Page 2, line 26: “the atmospheric number density”. I would suggest “the atmospheric number density of molecules”. Note that the pressure-to-temperature ratio would also do.

Done (page 2 line 26).

3. While the minimum height of measurements for the CHM15K instrument is indirectly given through its full overlap range, this information seems to be missing for the RALMO system. Even though the Raman technique employed in RALMO to derive the aerosol backscatter coefficient allows compensating incomplete overlap effects to some extent, I think RALMO’s minimum usable altitude should be stated for completeness.

Indeed, thanks to its Raman retrieval technique, the RALMO backscatter is unaffected by incomplete overlap issues. Nevertheless, the signal-to-noise is typically very low in the first 200 m above the station, hence this can be considered as a 'minimum usable altitude'. This information is now included in the manuscript (Page 3, Lines 28-30).

4. Note a possible inconsistence in the full overlap range of CHM15K. In line 4 of page 4 it is stated as “800 m above the station”, while in lines 2-3 of page 6 is it is said that “We only select measurements from ≈ 300 m above the ground station in order to minimize the effect a possible incomplete overlap of the lidar systems in the lower part of the profiles”. Left aside the already mentioned fact that no overlap information seems to be given for RALMO, do the authors use CHM15K data obtained below its full overlap range? This deserves some calrification.

Below the full overlap altitude of CHM15K (800 m above station), the backscatter profiles are corrected for the incomplete overlap between the incoming beam and the receiver’s field of view, as described in Hervo et al. (2016). This (previously missing) information is now included in the manuscript (Page 4, Line 9).
The rejection of all measurements below 300 m above the station is aimed to avoid the region of maximum incomplete overlap of CHM15K, as well as to avoid the region of low signal-to-noise ratio of RALMO at low altitudes (see answer to previous comment). This statement is now clarified in the manuscript (Page 6, Lines 23-25).

5. I suggest that a logarithmic scale be used for the horizontal axes in figs. 2a, b, and c. 6. In the caption of fig. 2 it should be stated that the graph in panel a is obtained for 3 -3 N=10 cm .Currently that information is found only in the main text. 7. I suggest trying to find a symbol (and give a name) for the ratio / β β aer mol . Otherwise the authors have to use the rather awkward notation BSR-1 to refer to that ratio and the text may even fall in ambiguities, for example in line 3 of page 8 when they say “Figure 2a shows the simulated aerosol backscatter ratio (i.e. BSR − 1)”. But the backscatter ratio is BSR, not BSR-1. Perhaps just / β β aer mol would do.

Done. The X-axis of Figure 2a-2b-2c (mode radius) was changed to logarithmic scale, and the information on number concentration (N = 10^3 cm^{-3}) was added to the caption of Figure 2. The notation 'BSR-1' was replaced with the more compact 'β_{aer}/β_{mol}' throughout Section 3.2 and in Figure 2.

<u>Anonymous Referee #2</u>

The manuscript shows an intercomparison between a Raman lidar, a commercial ceilometer and an optical in-situ sonde takes as reference. This contribution doesn't represent a substantial contribution to scientific progress and I agree that it is more indicated for Atmospheric Measurement Techniques than ACP.

Major Issues:

The FOV correction factor has been computed with a well defined aerosol distribution. How the results change if a more likely bi-modal distribution is used instead? Or changing the distribution width and/or the refractive index? As it is implemented, the correction is depending on a particular type of aerosol.

The single-lognormal size distribution assumed for the calculation of the FOV correction is to be interpreted as an *average* size distribution of boundary layer aerosols, rather than that of a well-defined population. This assumption has the advantage that the correction factors can be described as functions of a single parameter (R_m), which can be constrained through the observed AE, as discussed in Section 3.2. Assuming a more complex (e.g. bi-modal) size distribution, as well as relaxing one or more parameters of the size distribution (width, refractive index), would inevitably result in increased number of degrees of freedom of the correction factors, for which insufficient observational constraints are available. Therefore, the correction would be practically not applicable. In particular, for a bi-modal size distribution the correction factors would also depend on the number concentration (N) ratio of the two modes, whereas the correction for a single-lognormal distribution are independent of N.
Since furthermore, previous studies show that a mono-modal distribution represents well the average size distribution of continental aerosols in the Northern mid-latitudes (e.g., Watson-Perris et al., 2019), we believe the assumption of a single lognormal size distribution is justified. This choice is now motivated more carefully in the manuscript (Page 8, Lines 12-15), and a quantitative discussion of the uncertainty introduced by the FOV correction in the statistical comparison is now also provided in Section 4.3 (Page 15, Lines 12-15).

The statistical intercomparison is unclear and counter-intuitive. I would suggest to the authors to use the Pearson Cross Correlation coefficient paired with the Root Mean Square Error, on the whole atmospheric profile and at different altitude ranges, e.g. into the PBL, free troposphere...

Following this comment and one remark of Reviewer #2, the statistical comparison (including mainly Section 4 and Figures 5-10) has been strongly revised and improved. In particular, the following changes were made:

- Low and medium-high aerosol content measurements are separated according to an empirical threshold, and shown by different colors in Figures 5, 7, 8, 10.
- Mean and standard deviations profiles (Figures 5, 8) are calculated from medium-high aerosol content only, and the use of relative differences in the discussion is mainly restricted to medium-high aerosol content measurements.
- The probability density functions (Figures 6, 9) are calculated for medium-high aerosol content and all data separately.
- The Pearson correlation coefficient is now also calculated for medium-high aerosol content data, allowing to quantitatively evaluate the linearity of the correlation between the lidars and COBALD measurements.
- A new Section 3.3 (Page 9 Line 10 - Page 10 Line 17) was added to the manuscript, where we introduce the sorting of the data according to aerosol content, and formally define the compared quantities (Equations 3-6).

This approach allows to meaningfully quantify the deviations of medium-high aerosol content measurements at all altitudes, while at the same time not fully neglecting low aerosol content measurement in the free troposphere, and maintaining a clear and systematic structure. The Pearson correlation coefficient, evaluated for medium-high aerosol content data in three altitude intervals (0.8-3 km, 3-6 km, 0.8-6 km), adds a useful further insight to the characterization of the performances of the lidar instruments with respect to COBALD.
Given the similarity between the definitions of RSME and standard deviation (see Equation 5 in the manuscript), and the fact that standard deviation is predominantly used in previous aerosol backscatter intercomparison in the context of EARLINET (e.g., Matthais et al., 2004; Pappalardo et al., 2004), here we decide to keep standard deviation as a measure of variability. This choice also aims to avoid redundancy of information, which might turn out confusing for a reader (note that already three statistical parameters are used in this paper: mean deviation, standard deviation, and Pearson correlation coefficient, each of them quantified for different datasets and different altitude regions).
We believe the revised statistical comparison is strongly improved compared to the previous version of the paper, both in terms of scientific content and clarity, and we thank the reviewer for this comment.

Figure 5 and 8 are unnecessary.

Unfortunately, we are unable to understand properly this comment. Figures 5 and 8 show the vertical profiles of the RALMO – COBALD (Figure 5) and CHM15K – COBALD (Figure 8) difference in aerosol backscatter coefficient, which are a fundamental component of our statistical comparison. As discussed in the previous answer, Figures 5 and 8 were strongly improved in the revised version of the manuscript.

CHM15K inversion should be explained more in detail, as the molecular signal can be very low at 1064nm.

Using a similar ceilometer (CHM15kx by Jenoptik, Germany), Wiegner and Geiss (2012) show that a Klett inversion algorithm can provide accurate aerosol backscatter profiles, despite the low molecular backscatter at infrared wavelengths and the low signal-to-noise ratio in the free troposphere. This reference is now included in the manuscript (Page 4, Lines 11-13).

Optical measurements are strongly affected by water vapor absorption at 940nm. Usually, the ceilometers at this wavelength use a radiative transfer computation to correct the profile. What about COBALD sonde? In the text it is not mentioned.

The effect of water vapor absorption on COBALD BSR at 940 nm is negligible, due to the short optical path length of this instrument (≈ 10 m). COBALD uses two LEDs emitting 250 mW optical power and a detector with FOV of 6°. A good overlap between the emitted light beams and the detector FOV is established at ≈ 0.5 m distance from the sonde, and the backscattered signal from a distant layer decreases by the inverse distance squared. This means that, assuming uniform scattering conditions, the signal contribution at 10 m distance from the sonde falls below 0.25 % compared to that in the vicinity of the detector. In this sense, COBALD is considered as an *in-situ* instrument in this comparison.
Therefore, the uncertainty contribution associated with water vapor absorption at 940 nm on COBALD BSR is to be considered as included in the estimate of 5 % accuracy and 1 % precision provided by Vernier et al. (2015), now also given in the manuscript (Page 5, Lines 7-8).

Moreover, some equations are needed to better explain lines 25-28 (Pag. 4).

A new equation was added to define BSR (Equation 1), and the explanation has been broken in multiple sentences for more clarity (Page 5, lines 3-8).

It would be more interesting to intercompare the two instruments vs. COBALD for different meteorological conditions and aerosol loading.

We agree only in part with this comment. The performances of the analyzed instruments, both the lidars and COBALD, are to our best knowledge independent of meteorological conditions, hence we do not expect any systematic bias associated with meteorological parameters (such as temperature or specific humidity). Furthermore, our comparison already avoids all in-cloud and high RH measurements. This is done partly through the selection of the dataset (discussed in Section 2.3), where profiles for which a precise calibration of the lidar signal cannot be achieved are rejected (most frequently due to fog or low clouds), and subsequently through the rejection of all data points with RH > 90% in the statistical comparison (according to the radiosonde measurements) (see Page 7, Lines 1-3). Finally, the limited available dataset (17 soundings for RALMO vs. COBALD, 31 for CHM15K vs. COBALD), together with the irregular periodicity of COBALD soundings (see Table S1 in Supplementary material), and the strong day-to-day variability of boundary layer aerosols, do not allow for any robust investigation of seasonal patterns or other systematic weather-related behaviors.
On the other hand, our comparison does already take different aerosol loadings into account. This is done through the scatter plots of RALMO vs. COBALD β_{aer} (Figure 7) and CHM15K vs. COBALD β_{aer} (Figure 10), where their deviations are displayed and discussed as functions of the absolute COBALD β_{aer} signal, i.e. the aerosol loading (see in particular Page 13 Lines 15-18, Page 14 Lines 26-30). In the revised version of the manuscirpt, this aspect is further emphasized by the distinction between low and medium-high aerosol content measurements, now shown in different colors in Figures 5, 7, 8, 10, and evaluated separately in the statistical comparison (see Sections 3.3, 4.2, 4.3, and replies to comments above).

Validation of aerosol backscatter profiles from Raman lidar and ceilometer using balloon-borne measurements

Simone Brunamonti[1*], Giovanni Martucci[1], Gonzague Romanens[1], Yann Poltera[2], Frank G. Wienhold[2], Maxime Hervo[1], Alexander Haefele[1] and Francisco Navas-Guzmán[1]

[1]Federal Office of Meteorology and Climatology (MeteoSwiss), Payerne, Switzerland
[2]Swiss Federal Institute of Technology (ETH), Zürich, Switzerland
*Now at: Swiss Federal Laboratory of Material Sciences and Technology (Empa), Dübendorf, Switzerland

Correspondence to: Francisco Navas-Guzmán (francisco.navasguzman@meteoswiss.ch)

Abstract. Remote sensing measurements by light detection and ranging (lidar) instruments are fundamental for the monitoring of altitude-resolved aerosol optical properties. Here~~,~~ we validate vertical profiles of aerosol backscatter coefficient (β_{aer}) measured by two independent lidar systems using co-located balloon-borne measurements performed by Compact Optical Backscatter Aerosol Detector (COBALD) sondes. COBALD provides high-precision in-situ measurements of β_{aer} at two wavelengths (455 and 940 nm). The two analyzed lidar systems are the research Raman Lidar for Meteorological Observations (RALMO) and the commercial CHM15K ceilometer (Lufft, Germany). We consider in total 17 RALMO and 31 CHM15K profiles, co-located with simultaneous COBALD soundings performed throughout the years 2014-2019 at the MeteoSwiss observatory of Payerne (Switzerland). The RALMO (355 nm) and CHM15K (1064 nm) measurements are converted to respectively 455 nm and 940 nm using the Angstrom exponent profiles retrieved from COBALD data. To account for the different receiver field of view (FOV) angles between the two lidars (0.01-0.02°) and COBALD (6°), we derive a custom-made correction using Mie-theory scattering simulations~~.~~. Our analysis shows that both ~~RALMO and CHM15K~~lidar instruments achieve ~~a~~ on average a good agreement with COBALD measurements in the boundary layer and free troposphere, up to 6 km altitude~~, and including fine structures in the aerosol's vertical distribution~~. For medium-high aerosol content measurements at altitudes below 3 km, the mean ± standard deviation difference in β_{aer} calculated from all considered soundings is – 2 % ± 37 % (– 0.018 ± 0.237 Mm^{-1} sr^{-1} at 455 nm) for RALMO – COBALD, and + 5 % ± 43 % (+ 0.009 ± 0.185 Mm^{-1} sr^{-1} at 940 mm) for CHM15K – COBALD. Above 3 km altitude, absolute deviations generally decrease while relative deviations increase, due to the prevalence of air masses with low aerosol content. Uncertainties related to the FOV correction and spatial and temporal variability effects (associated with the balloon's drift with altitude and different integrations times) contribute to the large standard deviations observed at low altitudes. The lack of information on the aerosol size distribution and the high atmospheric variability prevent an accurate quantification of these effects. Nevertheless, the excellent agreement observed in individual profiles, including fine and complex structures in the β_{aer} vertical distribution, shows ~~that,~~ that under optimal conditions~~,~~ the discrepancies ~~between the two instruments~~with the in-situ measurements are typically ~~are typically~~ ~~smaller than~~comparable to the ~~the average of our statistical comparison~~estimated statistical uncertainties of the remote sensing measurements~~, the excellent agreement~~

~~observed in individual soundings shows that optimal conditions the discrepancies between the two instruments are typically much smaller than the standard deviations of our statistical comparison~~. Therefore, we conclude that β_{aer} profiles measured by the RALMO and CHM15K lidar systems are in good agreement with in-situ measurements by COBALD sondes up to 6 km altitude.

~~For altitudes below 2 km, the mean ± standard deviation difference in β_{aer} is + 6 % ± 40 % (+ 0.005 ± 0.319 Mm^{-1} sr^{-1}) for RALMO – COBALD at 455 nm, and + 13 % ± 51 % (+ 0.038 ± 0.207 Mm^{-1} sr^{-1}) for CHM15K – COBALD at 940 nm. The large standard deviations can be at least partly attributed to atmospheric variability effects, associated with the balloon's horizontal drift with altitude (away from the lidar beam) and the different integration times of the two techniques. Combined with the high spatial and temporal variability of atmospheric aerosols, these effects often lead to a slight altitude displacement between aerosol backscatter features that are seen by both techniques. For altitudes between 2-6 km, the absolute standard deviations of both RALMO and CHM15K decrease (below 0.13 and 0.16 Mm^{-1} sr^{-1}, respectively), while their corresponding relative deviations increase (often exceeding 100% COBALD of the signal). This is due to the low aerosol content (i.e. low absolute backscattered signal) in the free troposphere, and the vertically decreasing signal-to-noise ratio of the lidar measurements (especially CHM15K). Overall, we conclude that the β_{aer} profiles measured by the RALMO and CHM15K lidar systems are in good agreement with in-situ measurements by COBALD sondes up to 6 km altitude.~~

1. Introduction

Aerosol particles are ubiquitous in the atmosphere, and play a key role in multiple processes that affect weather and climate. They absorb and scatter the incoming and outgoing radiation, which affects the Earth's radiative budget (direct effect), and interact with cloud formation processes, influencing their microphysical properties and lifetime (indirect effect) (e.g., Haywood and Boucher, 2000). Atmospheric aerosols are one of the largest sources of uncertainty in current estimates of anthropogenic radiative forcing (Bindoff et al., 2013).

Among the most significant causes of this uncertainty is the high variability, in space and time, of the aerosol's concentration, composition and optical properties. Remote sensing instruments, such as light detection and ranging (lidar) systems, represent an optimal tool for the monitoring of altitude-resolved aerosol optical coefficients (backscatter and extinction), especially in the planetary boundary layer (PBL) (e.g., Amiridis et al., 2005; Navas-Guzmán et al., 2013). Lidar networks like EARLINET (www.earlinet.org) and E-PROFILE (www.eumetnet.eu/e-profile), comprising several hundreds of single-wavelength (including ceilometers) and multi-wavelength (Raman) lidars, provide a comprehensive database of the horizontal, vertical and temporal distribution of aerosols over Europe (e.g., Bösenberg et al., 2003; Pappalardo et al., 2014; Sicard et al., 2015).

Lidar instruments offer the advantages of vertically-resolved measurements and continuous operation in time, but are subject to a number of intrinsic uncertainties of this technique. Single-wavelength elastic backscatter lidars are limited by the fact that only one signal is measured, while the returning intensity is determined by two parameters (backscatter and extinction). Hence, an a-priori assumption on the aerosol extinction-to-backscatter ratio (the so-called 'lidar ratio') is necessary for the calculation of the aerosol backscatter profiles (e.g., Collis and Russel, 1976). Additionally, the retrieval at low altitudes is particularly challenging because of the incomplete geometric overlap between the incoming beam and the receiver's field of view (e.g., Wandinger and Ansmann, 2002; Weitkamp, 2005; Navas-Guzmán et al., 2011). The comparison of aerosol backscatter profiles from 19 elastic backscatter lidars in EARLINET found deviations within 10% in the PBL compared to more advanced Raman lidar measurements (Matthais et al., 2004).

Multi-wavelength Raman lidars allow the independent measurement of aerosol backscatter and extinction as functions of altitude, by the detection of a pure molecular backscatter signal in addition to the elastic backscatter (Ansmann et al., 1990; 1992). However, the retrieval procedure is complex and prone to uncertainties, in particular for extinction. It involves the calculation of the derivative of the logarithm of the ratio between the atmospheric number density of molecules and the lidar received power, which generally requires complex data handling techniques to isolate the signal from statistical fluctuations (Pappalardo et al., 2004). The comparison of different aerosol backscatter retrieval algorithms between 11 Raman lidar systems in EARLINET, using synthetic input data, showed deviations between them up to 20% for altitudes below 2 km (Pappalardo et al., 2004). This calls for careful validation studies against independent in-situ measurements, as we perform in this work.

In-situ instruments are characterized by higher precision and signal-to-noise ratio compared to remote sensing measurements, but are typically limited by low spatial and temporal coverage. Altitude-resolved in-situ measurements of aerosol optical properties can be achieved by various platforms including aircrafts, unmanned aerial vehicles (UAVs), and meteorological balloons. Specifically, balloon-borne measurements of aerosol backscatter are typically used to investigate high-altitude cirrus clouds (e.g., Khaykin et al., 2009; Cirisan et al., 2014) and aerosol layers in the upper troposphere and stratosphere (e.g., Rosen and Kjome, 1991; Vernier et al., 2015; Brunamonti et al., 2018), which are not accessible by aircrafts and UAVs. The aim of this paper is to use balloon-borne measurements of aerosol backscatter in the lower troposphere to validate the retrievals of aerosol backscatter coefficient by one co-located Raman lidar and one co-located ceilometer.

The instruments and data used for the comparison are introduced in detail in Section 2. The method of comparison, including the derivation of a field of view (FOV) correction from idealized Mie-theory scattering simulations, is described in Section 3. The results of the comparison are discussed in Section 4, and the conclusions summarized in Section 5.

2. Observations

We analyze vertical profiles of aerosol backscatter coefficient (β_{aer}) measured by two remote sensing instruments, namely one research Raman lidar system and one commercial ceilometer, and in-situ (balloon-borne) measurements performed by aerosol backscatter sondes. The three instruments and measuring techniques are introduced in Sections 2.1-2.2, and their main characteristics are summarized in Table 1. All data were collected at the MeteoSwiss Aerological Observatory of Payerne, Switzerland (46.82° N, 6.95° E), located at an elevation of 491 m above sea level (asl), between January 2014 and October 2019. The selection of the dataset considered for the statistical comparison is ~~discussed~~ described in Section 2.3. Spatial and temporal variability issues, related to the different characteristics of the lidar and balloon sounding techniques, are discussed in Section 2.4.

2.1. Remote sensing measurements

RALMO (Raman Lidar for Meteorological Observations) is a research Raman lidar system developed by EPFL Lausanne in collaboration with MeteoSwiss (Dinoev et al., 2013), operational in Payerne since 2008 and part of the EARLINET network. It uses a Nd:YAG laser source, which emits pulses of 8 ns duration at wavelength 355 nm and frequency of 30 Hz. The laser beam divergence is 120 µrad and the mean energy per pulse 400 mJ. The receiving system consists of four telescopes with 30 cm parabolic mirrors, with equivalent total aperture of 60 cm and field of view (FOV) angle of 200 µrad. Optical fibers connect the telescope mirrors with two polychromators, which allow to isolate the rotational-vibrational Raman signals of nitrogen and water vapor (wavelengths 386.7 nm and 407.5 nm, respectively) and the pure rotational Raman lidar signals (around 355 nm). The rotational-vibrational signals are used to derive water vapor profiles (Brocard et al., 2013; Hicks-Jalali et al., 2019; 2020), while the pure rotational signals are used for temperature, aerosol backscatter and aerosol extinction coefficients (e.g., Dinoev et al., 2010; Martucci et al., 2018). The optical signals are detected by photomultipliers and acquired by a transient recorder system (Brocard et al., 2013). Thanks to its Raman technique, RALMO retrievals are unaffected by incomplete overlap issues. Nevertheless, the signal-to-noise ratio is typically very low in the first 200 m above the station, therefore this altitude region is not considered in this study ~~(see Section 3.1)~~. Aerosol backscatter coefficient measurements from RALMO were recently used to characterize hygroscopic growth during mineral dust and smoke events (Navas-Guzmán et al., 2019). Here we derive the RALMO β_{aer} at 355 nm from the ratio between the elastic and inelastic signal, as described in Navas-Guzmán et al. (2019). The mean statistical uncertainties associated with the retrieval of β_{aer} at 355 nm from Raman inversion techniques are typically estimated as 15 % in the PBL (Pappalardo et al., 2004).

The CHM15K-Nimbus (hereafter CHM15K) ceilometer is a single-wavelength elastic backscatter lidar manufactured by Lufft, Germany (Lufft, 2019), installed in Payerne since 2012, and member of E-PROFILE. It uses a Nd:YAG narrow-beam micro-chip laser emitting 1 ns pulses at wavelength 1064 nm and repetition rate between 5-7 Hz, and a receiver FOV of 450 µrad. It supports a range up to 15 km with first overlap point at 80 m and full overlap reached at 800 m above the station (Hervo et al., 2016). Below this level, the profiles are corrected for incomplete overlap (~~as described in~~ Hervo et al., ~~(~~2016). CHM15K is employed as a cloud height sensor and for the automatic detection of boundary layer height (Poltera et al., 2017), and it was used for the characterization of aerosol hygroscopic properties (Navas-Guzmán et al., 2019). Here we derive β_{aer} at 1064 nm from the CHM15K elastic signal using ~~the~~ a Klett inversion ~~technique~~ algorithm (Klett, 1981~~).~~). This technique was shown to provide accurate aerosol backscatter profiles despite the low molecular backscatter at infrared wavelengths, and the low signal-to-noise ratio of a ceilometer in the free troposphere (Wiegner and Geiss, 2012). In particular, using a similar system (CHM15kx by Jenoptik, Germany), Wiegner and Geiss (2012) report a relative error of 10 % on β_{aer} at 1064 nm retrieved by

Formatiert: Englisch (Vereinigte Staaten)

Formatiert: Englisch (Vereinigte Staaten) this method. ~~F~~For consistency within ~~the~~ our statistical comparison, here we assume a constant lidar ratio equal to 50 sr for all profiles. The uncertainty related with this assumption will be discussed in Section 4.3.

2.2. In-situ measurements

COBALD (Compact Optical Backscatter Aerosol Detector) is a light-weight (500 g) aerosol backscatter detector for balloon-borne measurements developed at ETH Zürich, based on the original prototype by Rosen and Kjome (1991). Using two light emitting diodes (LEDs) as light sources and a photodiode detector with FOV of 6°, COBALD provides high-precision in-situ measurements of aerosol backscatter at wavelengths of 455 nm (blue visible) and 940 nm (infrared). COBALD was originally developed for the observation of high-altitude clouds, such as cirrus (e.g., Brabec et al., 2012; Cirisan et al., 2014) and polar stratospheric clouds (Engel et al., 2014), while recently it was proven able to detect and characterize aerosol layers in the upper troposphere ~~- and~~ lower stratosphere ~~-~~ (e.g., Vernier et al., 2015; 2018; Brunamonti et al., 2018). In this work, for the first time we use COBALD measurements for the analysis of boundary layer and lower tropospheric aerosols. ~~Here, for the first time we use COBALD measurements for the analysis of lower tropospheric aerosols.~~

For each balloon sounding, the COBALD sonde is connected to a host radiosonde via their XDATA interface (e.g., Wendell and Jordan, 2016) to transmit the data to the ground station. The average ascent rate of the balloon is set to around 5 m/s, which combined with a measurement frequency of 1 Hz, provides a vertical resolution of approximately 5 m. Typical balloon burst altitude is about 35 km. Due to the high sensitivity of its photodiode detector, COBALD sondes can be only deployed during night-time. Hence, all soundings analyzed here were started at approximately 23:00 UTC. More than 100 COBALD soundings were performed in Payerne since 2009, supported by SRS-C34 radiosondes by MeteoLabor, Switzerland (MeteoLabor, 2010) until December 2017, and RS41-SGP radiosondes by Vaisala, Finland (Vaisala, 2017) since January 2018.

The COBALD measurements are typically expressed as backscatter ratio (BSR) ~~at 455 and 940 nm~~, defined as the ratio of the total-to-molecular backscatter coefficient (Equation 1), at 455 and 940 nm. The BSR is obtained by dividing the total measured signal (normalized to the altitude-dependent LED emitted power) ~~signal~~ by its molecular contribution, which is computed from the atmospheric extinction according to Bucholtz (1995). The atmospheric number density of molecules is ~~and using air density~~ derived from the radiosonde measurements of temperature and pressure (e.g., Cirisan et al., 2014). Accuracy and precision of COBALD BSR were estimated by Vernier et al. (2015) as 5 % and 1 %, respectively, at upper tropospheric conditions. Here, we further derive β_{aer} from the COBALD BSR assuming a molecular extinction-to-backscatter ratio of 8π/3 sr.

$$BSR = \frac{\beta_{aer} + \beta_{mol}}{\beta_{mol}} \qquad \text{(Equation 1)}$$

Formatiert: Nicht Hervorheben

Formatiert: Nicht Hervorheben

Formatiert: Nicht Hervorheben

Formatiert: Einzug: Links: 4.99 cm

2.3. Dataset

Formatiert: Abstand Vor: 24 Pt.

Over their operational periods, the RALMO and COBALD systems were subject to various technical and design modifications, which affected their characteristics and performances. In particular, the currently used COBALD 940 nm LED was introduced in January 2014, replacing the older 870 nm LED (e.g., Brabec et al., 2012), while the pure rotational Raman acquisition board of RALMO was replaced, from a Licel system to the faster FAST ComTec P7888 (FastCom, Germany), in August 2015 (see Martucci et al., 2018). For consistency, we consider in this work only the time periods following these changes, i.e. the current versions of RALMO and COBALD up-to-date. Therefore, we analyze the years 2014-2019 for the CHM15K validation (58 total COBALD soundings), and the years 2016-2019 for the RALMO validation (34 total soundings: note that no simultaneous RALMO-COBALD soundings are available between August and December 2015).

Out of all the available COBALD soundings, we exclude those with simultaneously missing or incomplete (up to at least 6 km altitude) lidar profiles. This can be due to instrumental failures, maintenance interventions, or forbidding weather conditions (e.g. thick low clouds, fog or precipitation) at the time of the ~~COBALD~~ balloon sounding. In particular, we reject from the comparison all profiles for which a precise calibration of the lidar signal cannot be achieved. The calibration of lidar (as well as COBALD) measurements involves the normalization of the signal to a reference value in a 'clean region' (i.e. the lowest aerosol concentration along the profile), usually found in the upper troposphere. If no lidar signal is measured in this region of altitudes, which is typically the case in the presence of thick low clouds, or if the signal-to-noise ratio above the cloud is so low that the signal cannot be properly calibrated, then the profile is excluded from the comparison. After a careful selection, we obtain 17 simultaneous calibrated profiles of RALMO and COBALD and 31 of CHM15K and COBALD, which are used for the statistical comparison. The list of corresponding dates is given by Table S1 in Supplementary material.

2.4. Spatial and temporal variability

A fundamental difference between the remote sensing and balloon sounding techniques is that lidars measure at every altitude the vertical air column directly above their laser beam, while the balloon sondes are subject to a horizontal drift with altitude, dictated by the atmospheric wind field. Therefore, in presence of wind shear, the two instruments may not measure the same air mass at every altitude. The distance between the balloon sonde and the lidar beam generally increases with altitude, and is strongly dependent on the atmospheric wind profile at the time of measurement. Figure 1 shows the trajectories of all balloon soundings analyzed in our comparison for the period 2016-2019, as function of altitude (0.8-6 km). The distance between the lidar and the sondes ranges between roughly 0-5 km up to 2 km altitude, and may exceed 10 km at 4 km altitude.

In addition, the two techniques differ in terms of measurement times. Namely, while the lidar profiles are integrated 30 min in time, COBALD provides instantaneous measurements at 1 s resolution (reduced to 6 s after averaging to 30 m intervals). The combination of balloon drift with altitude and different integration times, coupled with the high spatial and temporal variability of aerosol optical properties, can lead to discrepancies between the remote sensing and in-situ measurement which are not due to instrumental issues, but rather to atmospheric variability effects. In particular, this may result in the smoothing or slight displacement in altitude between aerosol backscatter features (especially thin layers), which are seen by both techniques. Such effects are often observed in our dataset, and therefore affect the results of the statistical comparison. This issue will be discussed further in Section 4.3.

3. Method of comparison

For each COBALD sounding, we retrieve simultaneous RALMO and CHM15K β_{aer} profiles with vertical resolution of 30 m and integration time of 30 min (roughly corresponding to 10 km of balloon ascent time). Since all COBALD sondes were launched at 23:00 UTC, the integration time window chosen for all profiles and both lidars is 23:00-23:30 UTC. To obtain a dataset with consistent vertical levels, the COBALD measurements (with vertical resolution ≈ 5 m) are averaged in altitude bins of 30 m, matching the vertical grid of the lidars. For the statistical comparison we consider in total 174 vertical levels, covering the altitude interval from 800 m asl to 6 km asl. We only select measurements from ≈ 300 m above the ground station to avoid the region of maximum ~~uncertainty of the~~incomplete overlap ~~correction~~ of CHM15K, as well as to avoid the region of low signal-to-noise ratio of RALMO at low altitudes ~~minimize the effect a possible incomplete overlap of the lidar systems in the lower part of the profiles~~(see Section 2.1). ~~(n~~Note that all altitude levels given in the following are meant as altitude asl, unless differently specified~~)~~.

Along with the COBALD backscatter data, the temperature, pressure and relative humidity (RH) measurements from the host radiosonde are averaged to the same altitude levels. The temperature and pressure profiles are used for the computation of the atmospheric molecular extinction, as described in Section 2.2. The RH measurements are used to reject in-cloud data points. In-cloud aerosol backscatter measurements are typically much larger (up to three orders of magnitude) compared to clear-sky (i.e. aerosol-only) conditions, and characterized by high spatial and temporal variability. Therefore, we exclude from the comparison all data points with RH > 90%. Such a highly conservative criterion is chosen in order to avoid as well cloud edge regions, which can lead to large biases in the statistical comparison.

For a proper comparison of the ~~remote sensing and balloon-borne measurements~~COBALD and lidar backscatter retrievals, a number of methodological aspects and technical differences between the ~~lidar and COBALD instruments~~two techniques need to be taken into account. ~~Here we~~In the remainder of this section, we discuss our approach towards ~~spatial and temporal variability issues (Section 3.1),~~ wavelength homogenization (Section 3.~~2~~1), ~~and~~ correction of effects related to the different receiver FOVs (Section 3.~~3~~2), data sorting according to aerosol content and compared quantities (Section 3.3)~~.~~.

3.1. ~~Spatial and temporal variability~~ Wavelength conversion

~~For each COBALD sounding, we retrieve simultaneous RALMO and CHM15K profiles with vertical resolution of 30 m and integration time of 30 min (roughly corresponding to 10 km of balloon ascent time). Since all COBALD sondes were launched~~

Formatiert: Schriftart: Nicht Kursiv

~~at 23:00 UTC, the integration time window chosen for all profiles and both lidars is 23:00-23:30 UTC. To obtain a dataset with consistent vertical levels, the COBALD measurements (with vertical resolution ≈ 5 m) are averaged in altitude bins of 30 m, matching the vertical grid of the lidars. For the statistical comparison we consider in total 174 vertical levels, covering the altitude interval from 800 m asl to 6 km asl. We only select measurements from ≈ 300 m above the ground station in order to minimize the effect a possible incomplete overlap of the lidar systems in the lower part of the profiles. Note that all altitude levels given in the following are meant as altitude asl, unless differently specified.~~

~~Along with the COBALD backscatter data, the temperature, pressure and relative humidity (RH) measurements from the host radiosonde are averaged to the same altitude levels. The temperature and pressure profiles are used for the computation of the atmospheric molecular extinction, as described in Section 2.2. The RH measurements are used to reject in-cloud data points. In-cloud aerosol backscatter measurements are typically much larger (up to three orders of magnitude) compared to clear-sky (i.e. aerosol-only) conditions, and characterized by high spatial and temporal variability. Therefore, we exclude from the comparison all data points with RH > 90%. Such a highly conservative criterion is chosen in order to avoid as well cloud edge regions, which can lead to large biases in the statistical comparison.~~

~~A fundamental difference between the remote sensing and balloon sounding techniques is that lidars measure at every altitude the vertical air column directly above their laser beam, while the balloon sondes are subject to a horizontal drift with altitude, dictated by the atmospheric wind field. Therefore, in presence of wind shear, the two instruments may not measure the same air mass at every altitude. The distance between the balloon sonde and the lidar beam generally increases with altitude, and is strongly dependent on the atmospheric wind profile at the time of measurement. Figure 1 shows the trajectories of all balloon soundings analyzed in our comparison for the period 2016-2019, as function of altitude (0.8-6 km). The distance between the lidar and the sondes ranges between roughly 0-5 km up to 2 km altitude, and may exceed 10 km at 4 km altitude.~~

~~In addition, the two techniques differ in terms of measurement times. Namely, while the lidar profiles are integrated 30 min in time, COBALD provides instantaneous measurements at 1 s resolution (reduced to 6 s after averaging to 30 m intervals). The combination of balloon drift with altitude and different integration times, coupled with the high spatial and temporal variability of aerosol optical properties, can lead to discrepancies between the remote sensing and in-situ measurement which are not due to instrumental issues, but rather to atmospheric variability effects. In particular, this may result in the smoothing or slight displacement in altitude between aerosol backscatter features (especially thin layers) which are seen by both techniques. Such effects are often observed in our dataset (see Section 4.1) and are not corrected in the statistical comparison, hence they contribute to increasing the standard deviation of the results.~~

~~3.2. Wavelength conversion~~

To compare β_{aer} at different wavelengths (λ) measured by the different instruments, it is necessary to account for the spectral dependency of aerosol backscatter. This ~~can be~~is done using the Angstrom law (Equation ~~1~~2), which describes the spectral dependency of β_{aer} between two wavelengths (λ_0 and λ) as function of the Angstrom exponent (AE) at every altitude level (z_i).

Formatiert: Tiefgestellt

The AE is an intensive property of the aerosol that, under certain assumptions on the particle's size distribution, can be used as a semi-quantitative indicator of particle size (e.g., Njeki et al., 2012; Navas-Guzmán et al., 2019). Through Equation ~~1~~ 2 we convert the lidar profiles into the COBALD wavelengths, so they can be quantitatively compared.

$$\beta_{aer}(\lambda, z_i\cancel{z}) = \beta_{aer}(\lambda_0, z_i\cancel{z}) \cdot \left(\frac{\lambda}{\lambda_0}\right)^{-AE(z_i\cancel{z})} \qquad \text{(Equation } \cancel{1}2\text{)}$$

Thanks to its high signal-to-noise ratio and two operating wavelengths, COBALD allows to characterize the backscatter spectral ratio (between 455 nm and 940 nm) at every altitude, including regions of low aerosol load (e.g., Brunamonti et al., 2018). Conversely, the signal-to-noise ratio of remote sensing instruments (in our case especially CHM15K) decreases with altitude, and the AE derived from lidar measurements is typically characterized by large statistical fluctuations in the free troposphere. Therefore, here we choose to retrieve the AE(z) profiles from COBALD data. To minimize the uncertainty associated with the conversion, we couple each lidar with the closest COBALD channel in terms of wavelength. Hence, the RALMO profiles at 355 nm (ultraviolet) are converted to 455 nm and compared to the COBALD blue visible channel, and the CHM15K profiles at 1064 nm (infrared) are converted to 940 nm and compared to the COBALD infrared channel.

Using the AE from COBALD is equivalent to assuming that the spectral behavior of the aerosols between 455-940 nm can be extrapolated to the slightly broader interval of 355-1064 nm, which is justified by the small difference between the wavelengths that are compared. A number of sensitivity tests using different assumptions have been conducted, revealing that small changes in AE have a small effect on the results. The uncertainty associated with the wavelength conversion of the lidar data is discussed further in ~~the conclusions (~~Section ~~5~~4.3)~~. (e.g., less than 2% change in β_{aer} for a 10% change in AE, for 455 nm and AE ≈ 1). In particular, the entire statistical comparison discussed in Section 4.2.1, using AE profiles from COBALD, was repeated using AE profiles derived from RALMO and CHM15K measurements, and assuming a constant AE = 1 for all altitudes. The results are displayed in Figure S1 in Supplementary material and show no relevant variations.~~

3.~~3~~2. Field of View (FOV) correction

Besides their wavelengths, the COBALD and lidar systems differ in terms of field of view (FOV) of their respective receivers. RALMO and CHM15K use highly focused laser beams, and consequently have narrow FOVs (200 µrad and 450 µrad, respectively, corresponding to 0.01-0.02°), while COBALD's photodiode detector has a macroscopic FOV of 6° (see Table 1). Considering that the Mie-scattering phase function, i.e. the distribution of scattered light with angle by a spherical particle, has a local maximum in the backward direction (180°), it follows from its wider FOV that COBALD will measure less backscattered radiation (namely, the average intensity between 174°-180°) compared to the lidars (≈ 180°).

Formatiert: Schriftart: Nicht Kursiv, Nicht Hervorheben

Formatiert: Schriftart: Nicht Kursiv, Nicht Hervorheben

Formatiert: Schriftart: Nicht Kursiv, Nicht Hervorheben

Formatiert: Schriftart: Nicht Kursiv, Nicht Hervorheben

To quantify this effect, we performed idealized Mie-theory scattering simulations using the optical model by Luo et al. (2003). We assume a single lognormal size distribution of aerosol particles characterized by mode radius R_m, number concentration N, fixed width (~~σ =~~ standard deviation 1.4)~~,~~ and refractive index (1.4)~~. Then, the~~ The BSR of this population is then computed both assuming the phase function value at 180°, corresponding to the lidar observations (FOV ≈ 0°), and taking the average of the phase function between angles 174°-180°, corresponding to the COBALD measurements (FOV = 6°). ~~The results are presented in Figure 2.~~ The use of a mono-modal size distribution with fixed width has the advantage that the correction factors can be described as functions of a single parameter (R_m), which can be constrained through the observed AE. Furthermore, a mono-modal distribution represents well the average size distribution of continental aerosols in the Northern mid-latitudes (e.g., Watson-Perris et al., 2019).

Figure 2a shows the simulated ratio of aerosol-to-molecular backscatter coefficient, β_{aer} ~~aerosol~~ /β_{mol} ~~backscatter ratio~~ (i.e., BSR ~~=~~ – 1; see Equation 1) at 455 nm (blue) and 940 nm (red), as function of R_m (40 nm-4 µm), calculated assuming FOV ≈ 0° (solid lines) and FOV = 6° (dashed lines), ~~as function of R_m for the interval 10 nm - 4 µm,~~ and $N = 10^3$ cm^{-3}. As expected, the simulations show that for all mode radii the COBALD β_{aer} ~~BSR~~ is lower than ~~the~~ the β_{aer} ~~BSR~~ measured by the lidar instruments ~~(Figure 2a)~~. Figure 2b shows the lidar-to-COBALD ratio of β_{aer} ~~BSR – 1~~ (ratio of solid-to-dashed curves in Figure 2a), i.e. the correction factor required to compensate for ~~this~~ the FOV effect, for 455 and 940 nm as function of R_m~~.~~. ~~(note that β_{aer} is proportional to BSR – 1, so that this ratio corresponds to the correction factor for β_{aer}).~~ For the considered size interval ~~of mode radii~~, the correction factors vary between approximately 1-1.5 and show a non-linear dependency on R_m, with a local maximum near ~~R_m ≈~~ 800 nm (λ = 455 nm) and ~~R_m ≈~~ 1.6 µm (λ = 940 nm). This complex optical behavior needs to be corrected. Note that the correction factors in Figure 2b are independent of N, unlike the β_{aer}/β_{mol} ratios ~~BSR~~ in Figure 2a.

To account for the size-dependency in Figure 2b, we use the AE as an indicator of particle size, and develop a parametrization of the correction factors based on the AE measured from COBALD. Figure 2c shows AE between 455-950 nm calculated from the Mie simulations, as function of R_m. The AE decreases non-monotonically with mode radius and exhibits the characteristic Mie oscillations in the range of approximately ~~20~~ 40 nm - 1 µm (Figure 2c). More in detail, we observe that AE > 1.5 corresponds to small particles (R_m < 75 nm), AE < 0.8 to large particles (R_m > 1.16 µm), while 0.8 < AE < 1.5 corresponds to 75 nm < R_m < 1.16 µm, but in this intermediate range the change of AE with R_m is not monotonic (Figure 2c), hence a one-to-one correspondence cannot be established. To simplify this behavior, we ~~choose to~~ parametrize the correction factors within the three fixed intervals of AE just introduced, and for each interval of AE we take the average correction factor in the corresponding interval of R_m. Hence, ~~for all measurements with 0.8 < AE < 1.5~~ we apply the average correction factors between 75 nm - 1.16 µm (namely, 1.23 at 455 nm, 1.10 at 940 nm) to all measurements with 0.8 < AE < 1.5~~)~~, ~~for AE < 0.8~~ the average correction factors between 1.16 - 4 µm (1.29 at 455 nm, 1.28 at 940 nm) for AE < 0.8, and no correction for AE > 1.5 (both correction factors ≈ 1 for R_m < 75 nm) ~~we do not apply any correction (both correction factors ≈ 1 for R_m < 75 nm)~~. The resulting FOV correction as function of AE is shown in Figure 2d.

The FOV correction ~~shown in Figure 2d~~ is applied to all COBALD measurements in the statistical comparison. Since, for every AE, the correction factors are larger for 455 nm than for 940 nm (Figure 2d), the FOV correction will affect the RALMO

Formatiert: Schriftart: Nicht Kursiv

Formatiert: Schriftart: Nicht Kursiv

Formatiert: Englisch (Vereinigtes Königreich)

Formatiert: Englisch (Vereinigtes Königreich)

Formatiert: Englisch (Vereinigtes Königreich) comparison more than ~~for~~ the CHM15K one. We note that, due to the variability of AE observed in our dataset (see Figure ~~S2~~ S1 in Supplementary material), the middle interval of the correction (0.8 < AE < 1.5) accounts for the large majority of data points in the PBL, AE > 1.5 typically corresponds to free tropospheric background measurements, which are unaffected by the correction, while values of AE < 0.8, corresponding to very large particles, are rarely encountered in our dataset. The effect of the FOV correction on two ~~individual~~ selected profiles ~~and the statistical comparison is~~will be discussed ~~further~~ in ~~the next~~ ~~s~~Section 4.1.

3.3. Compared quantities

After the wavelength conversion and the ~~application of the~~ FOV correction, ~~,~~

the difference ~~(δ_i)~~ in aerosol backscatter coefficient ($\Delta\beta_{aer}$) between the lidars (*LID*) and COBALD (*COB*) is calculated for ~~every~~each sounding and every ~~each~~ altitude level ~~(z_i)~~ (as in Equation ~~2~~3)~~:~~. The mean deviation (δ) ~~in given altitude layer and~~ of a given subset of data is calculated according to Equation 4, where z_1~~, …~~ … ~~,~~ z_N ~~represents~~ is the ensemble of all vertical levels in the considered ~~profiles~~ dataset and altitude region. The spread of the individual differences around δ is quantified using standard deviation (σ), defined by Equation 5. Mean and standard deviations are expressed both in absolute backscatter coefficient units (Mm^{-1} sr^{-1}) and in percent units relative to the COBALD signal.

$$\Delta\beta_{aer}(z_i) = \beta_{aer}^{LID}(z_i) - \beta_{aer}^{COB}(z_i) \qquad \text{(Equation 3)}$$

~~ensemble of is calculated according to Equation 3~~

$$\delta = \frac{\sum_{i=1}^{N} \Delta\beta_{aer}(z_i)}{N} \qquad \text{(Equation 4)}$$

~~wnote that the same definition applies for the calculation of the average difference at a given altitude level between all soundings, as well as for the average for a single sounding).~~

~~The variability of all deviations with respect to Δ in the considered ensamble is quantified throught the standard deviation (σ), calculated according to Equation 4:~~

$$\sigma = \sqrt{\frac{\sum_{i=1}^{N} (\Delta\beta_{aer}(z_i) \cancel{\delta_i} - \delta \cancel{\Delta})^2}{N-1}} \qquad \text{(Equation } \cancel{5}4)$$

Formatiert: Einzug: Links: 0 cm, Hängend: 1.25 cm

Formatiert: Schriftart: Kursiv, Tiefgestellt

Formatiert: Abstand Nach: 12 Pt.

Formatiert: Schriftart: Kursiv

Formatiert: Einzug: Links: 3.75 cm, Abstand Vor: 0 Pt.

Formatiert: Abstand Nach: 6 Pt.

Formatiert: Schriftart: 11 Pt.

Formatiert: Schriftart: 11 Pt.

Formatiert: Schriftart: 11 Pt.

Formatiert: Schriftart: 11 Pt.

Formatiert: Schriftart: 11 Pt.

Formatiert: Schriftart: 11 Pt.

Formatiert: Schriftart: 11 Pt.

Formatiert: Schriftart: 11 Pt.

Formatiert: Schriftart: 11 Pt.

Formatiert: Schriftart: 11 Pt.

Formatiert: Schriftart: 11 Pt.

Formatiert: Schriftart: Kursiv

Formatiert: Abstand Vor: 0 Pt., Nach: 18 Pt.

Formatiert: Schriftart: 11 Pt.

Formatiert: Schriftart: 11 Pt.

Formatiert: Schriftart: 11 Pt.

Formatiert: Schriftart: 11 Pt.

Formatiert: Schriftart: 11 Pt.

Formatiert: Schriftart: 11 Pt.

Formatiert: Schriftart: 11 Pt.

Formatiert: Schriftart: 11 Pt.

Formatiert: Schriftart: 11 Pt.

Formatiert: Schriftart: 11 Pt.

Formatiert: Schriftart: 11 Pt.

Formatiert: Schriftart: 11 Pt.

Formatiert: Schriftart: 11 Pt.

~~In a typical a~~Atmospheric backscatter profile~~s, a~~are typically characterized by a large gradient in β_{aer} between the boundary layer, with high aerosol content (hence high β_{aer}), and the free troposphere, with low aerosol content (low β_{aer}). This gradient is such that the same absolute $\Delta\beta_{aer}$ may correspond to either a small or large relative $\Delta\beta_{aer}$, depending on altitude. In particular, free tropospheric measurements, where statistical fluctuations often dominate over the atmospheric signal, typically yield large relative deviations in spite of small absolute differences. While the boundary layer is the main region of the interest of this study, as it contains most of the aerosol loading in the column, the free troposphere (including low aerosol content measurement) cannot be completely neglected, since a good agreement at high altitudes ensures that all profiles are well calibrated (see Section 2.3). Therefore, here we focus our analysis on medium-high aerosol content data (defined as explained below), yet for completeness we also display low aerosol content measurements in the statistical comparison. ~~all~~

The aerosol content is evaluated according to the average COBALD β_{aer} in each profile and 300 m altitude interval (i.e., mean of 10 vertical levels). Based on the observed range of variability of β_{aer} in our dataset (see Figures S1 supplementary material), we define 'low aerosol content' all layers with average COBALD $\beta_{aer} < 0.1$ Mm^{-1} sr^{-1} at 455 nm (RALMO comparison), and average COBALD $\beta_{aer} < 0.05$ Mm^{-1} sr^{-1} at 940 nm (CHM15K comparison). The averaging in 300 m layers ensures that actual air masses with low aerosol content are identified, rather than individual data points exceeding the threshold due to statistical variability. When the above conditions are met, all data points in the considered layer are classified as 'low aerosol content'. All other data points are referred to as 'medium-high aerosol content'. Note that this definition allows individual data points to exceed the threshold, as long as the average criteria in the layer are not exceeded.

For medium-high aerosol content data,

~~Finally~~in addition to δ and σ, we also evaluate ~~,~~ the correlation between ~~the lidars~~the lidars and ~~and~~ COBALD ~~is evaluated through~~using the Pearson correlation coefficient (ρ)~~,~~. This is ~~defined~~defined according to Equation ~~5~~6, where B_{LID} and B_{COB} are respectively the average lidar β_{aer} and COBALD β_{aer}, calculated in 300 m layers. The Pearson correlation coefficient represents the degree of linearity of the correlation between β_{aer}^{LID} and β_{aer}^{COB}, ranging between values of -1 (total negative linear correlation) and +1 (total positive linear correlation). In the statistical comparison, δ, σ, and ρ are quantified for both RALMO and CHM15K in three altitude intervals of 0.8-3 km asl, 3-6 km asl, and 0.8-6 km asl (i.e., all altitudes). ~~:~~

$$\rho = \frac{\sum_{i=1}^{N}\left(\beta_{aer}^{LID}(\cancel{\lambda,}z_i)-B_{LID}\right)\cdot\left(\beta_{aer}^{COB}(\cancel{\lambda,}z_i)-B_{COB}\right)}{\sqrt{\sum_{j=1}^{N}\left(\beta_{aer}^{LID}(\cancel{\lambda,}z_i)-B_{LID}\right)^2\cdot\sum_{k=1}^{N}\left(\beta_{aer}^{COB}(\cancel{\lambda,}z_i)-B_{COB}\right)^2}}$$

(Equation ~~5~~6)

~~Where B_{LID} and B_{COB} are the average lidar and COBALD β_{aer} in the considered ensemble of data: $B_{LID} = \frac{\sum_{i=1}^{N}\beta_{aer}^{LID}(\lambda,z_i)}{N}$ (Equation 6)~~

Formatiert: Abstand Vor: 0 Pt.

Formatiert: Schriftart: Kursiv

Formatiert ...

Formatiert: Block, Einzug: Links: 0 cm, Erste Zeile: 0 cm, Abstand Vor: 0 Pt., Nach: 0 Pt.

Formatiert ...

Formatiert ...

Formatiert: Einzug: Links: 0 cm, Erste Zeile: 0 cm, Abstand Vor: 0 Pt., Nach: 0 Pt.

Formatiert: Einzug: Links: 2.5 cm, Erste Zeile: 1.25 cm, Abstand Vor: 12 Pt.

Formatiert: Schriftart: 11 Pt.

Formatiert ...

Formatiert: Einzug: Links: 4.99 cm, Erste Zeile: 1.25 cm, Abstand Nach: 6 Pt.

Formatiert ...

Formatiert ...

$$\cancel{B_{COB} = \frac{\sum_{i=1}^{N} \beta_{aer}^{COB}(\lambda, z_i)}{N}} \qquad \text{~~(Equation 7)~~}$$

~~The Pearson correlation coefficient represents the degree of linear correlation of β_{aer} between the lidars and COBALD, ranging between values of -1 (total negative linear correlation) to +1 (total positive linear correlation).Mean and standard deviations are expressed in absolute backscatter coefficient values (units of Mm^{-1} sr^{-1}) as well as in percent units relative to the COBALD signal (Equations 8, 9):~~

$$\cancel{\Delta_{rel} = \frac{1}{N} \sum_{i=1}^{N} \frac{\delta_i}{\beta_{aer}^{COB}(z_i)}} \qquad \text{~~(Equation 8)~~}$$

$$\cancel{\sigma_{rel} = \sqrt{\frac{1}{N-1} \sum_{i=1}^{N} \frac{(\delta_i - \Delta)^2}{\beta_{aer}^{COB}(z_i)}}} \qquad \text{~~(Equation 9)~~}$$

~~A common issue when comparing aerosol backscatter coefficients~~

~~A fundamental difference between the remote sensing and balloon sounding techniques is that lidars measure at every altitude the vertical air column directly above their laser beam, while the balloon sondes are subject to a horizontal drift with altitude, dictated by the atmospheric wind field. Therefore, in presence of wind shear, the two instruments may not measure the same air mass at every altitude. The distance between the balloon sonde and the lidar beam generally increases with altitude, and is strongly dependent on the atmospheric wind profile at the time of measurement. Figure 1 shows the trajectories of all balloon soundings analyzed in our comparison for the period 2016-2019, as function of altitude (0.8-6 km). The distance between the lidar and the sondes ranges between roughly 0-5 km up to 2 km altitude, and may exceed 10 km at 4 km altitude.~~

~~In addition, the two techniques differ in terms of measurement times. Namely, while the lidar profiles are integrated 30 min in time, COBALD provides instantaneous measurements at 1 s resolution (reduced to 6 s after averaging to 30 m intervals). The combination of balloon drift with altitude and different integration times, coupled with the high spatial and temporal variability of aerosol optical properties, can lead to discrepancies between the remote sensing and in-situ measurement which are not due to instrumental issues, but rather to atmospheric variability effects. In particular, this may result in the smoothing or slight displacement in altitude between aerosol backscatter features (especially thin layers) which are seen by both techniques. Such effects are often observed in our dataset (see Section 4.1) and are not corrected in the statistical comparison, hence they contribute to increasing the standard deviation of the results.~~

- **Formatiert:** Nicht Hervorheben
- **Formatiert:** Einzug: Links: 4.99 cm, Abstand Vor: 0 Pt., Nach: 6 Pt.
- **Formatiert:** Nicht Hervorheben
- **Formatiert:** Einzug: Links: 4.99 cm, Erste Zeile: 1.25 cm, Abstand Nach: 6 Pt.
- **Formatiert:** Schriftart: 11 Pt.
- **Formatiert:** Schriftart: 11 Pt.
- **Formatiert:** Schriftart: 11 Pt.
- **Formatiert:** Einzug: Links: 4.99 cm, Erste Zeile: 1.25 cm, Abstand Vor: 24 Pt.
- **Formatiert:** Schriftart: 11 Pt.
- **Formatiert:** Schriftart: 11 Pt.
- **Formatiert:** Schriftart: 11 Pt.
- **Formatiert:** Schriftart: 11 Pt.
- **Formatiert:** Schriftart: 11 Pt.
- **Formatiert:** Schriftart: 11 Pt.
- **Formatiert:** Schriftart: 11 Pt.
- **Formatiert:** Schriftart: 11 Pt.
- **Formatiert:** Schriftart: 11 Pt.
- **Formatiert:** Schriftart: 11 Pt.
- **Formatiert:** Schriftart: 11 Pt.
- **Formatiert:** Schriftart: 11 Pt.
- **Formatiert:** Schriftart: 11 Pt.
- **Formatiert:** Schriftart: 11 Pt.
- **Formatiert:** Schriftart: 11 Pt.
- **Formatiert:** Einzug: Links: 0 cm, Erste Zeile: 0 cm, Abstand Nach: 0 Pt.
- **Formatiert:** Abstand Vor: 24 Pt.
- **Formatiert:** Abstand Nach: 12 Pt.
- **Formatiert:** Abstand Vor: 24 Pt., Nach: 12 Pt.

4. Results

Formatiert: Abstand Vor: 24 Pt.

In this section we present the results of our analysis. Before the statistical comparison (Section 4.2), we discuss the comparison of two selected individual profiles (Section 4.1), highlighting the effect of the FOV correction. Finally, the results are discussed in Section 4.3. ~~Note that two~~ Two additional examples of individual profiles can be found in Supplementary material (Figures ~~S3~~S2-S3~~4~~).

4.1. Comparison of individual profiles

To illustrate the main characteristics of the observed β_{aer} profiles and the effect of the FOV correction, we select ~~select two individual cases corresponding to the COBALD soundings made~~as case studies the soundings performed on 12 July 2018 and 4 September 2018. Figure 3 shows an overview of these measurements, including vertical profiles of β_{aer} (at different λ) by RALMO, COBALD and CHM15K (~~panels~~ Panels a, d), AE derived from COBALD measurements (~~panels~~ Panels b, e), plus the temperature and RH profiles measured by the radiosonde (~~panels~~ Panels c, f), ~~for~~ as functions of ~~the~~ altitude for the interval of 0.8-6 km asl.

The case of 12 July 2018 (Figure 3~~, top row~~a-c) shows a typical profile with top of PBL at about 2.2 km altitude (see temperature inversion, Panel c), characterized by a sharp decrease with altitude in β_{aer} and RH, plus a thin (≈ 400 m) isolated aerosol layer around 3 km altitude (note the higher AE compared to the PBL, suggesting finer particles: Panel b). Inside the PBL, the vertical structure of β_{aer} observed by COBALD is qualitatively well reproduced by both RALMO and CHM15K, despite an evident altitude displacement (of about 60 m) of the top-of-PBL decrease in β_{aer} between the COBALD and lidar profiles (Figure 3a). This is most likely an effect of the atmospheric variability issues discussed in Section 2~~3~~.4~~1~~. Indeed, considering that COBALD crosses the PBL around the beginning of the lidar integration time window, a downward displacement in top of PBL altitude (as inferred from the β_{aer} profiles) in the remote sensing data is consistent with the lowering of PBL altitude during nighttime reported by Poltera et al. (2017). A similar feature can be seen in Figure ~~S3d~~ S2d in Supplementary material.

On 4 September 2018 (Figure 3d-f~~, bottom row~~) a more complex aerosol vertical distribution is observed, with decreasing β_{aer} with altitude until 2 km, and a thick aerosol layer between 2.5-3.5 km altitude. Again, the vertical structure of β_{aer} observed by COBALD is ~~qualitatively~~ very well reproduced by both remote sensing products throughout the entire analyzed altitude range, including both aerosol layers inside and above the PBL. In this case, no significant altitude displacement is observed between the β_{aer} features of the COBALD and remote sensing profiles (Figure 3d).

Figure 4 shows the results of the quantitative comparison for the two cases just discussed, meaning the β_{aer} profiles obtained after converting the lidar wavelengths (355 to 455 nm and 1064 to 940 nm) and applying the FOV correction to the COBALD measurements. In particular, Figure 4 shows vertical profiles of β_{aer} at 455 nm from RALMO and COBALD (Panels a, e), β_{aer} at 940 nm from CHM15K and COBALD (Panels c, g), and their respective differences ($\Delta\beta_{aer}$) at 455 nm (Panels b, f) and 940 nm (Panels d, h), for 12 July 2018 (Panels a-d) and 4 September 2018 (Panels e-h). The COBALD β_{aer} and $\Delta\beta_{aer}$ profiles are shown both before (dashed lines) and after (solid lines) the FOV correction.

The FOV correction significantly improves the agreement between RALMO and COBALD measurements. Before the ~~FOV~~ correction (dashed lines), the RALMO profiles are characterized by a systematic high bias with respect to COBALD, ~~in the PBL,~~ of about 0.2 Mm^{-1} sr^{-1} in the PBL ~~for $z < 2$ km~~ (Figures 4a-b, 4e-f). After the FOV correction (solid lines), which increases the COBALD β_{aer} by a factor of 1.23 in this region of altitudes (see Figure 2d and AE profiles in Figure 3b), the discrepancy with RALMO is drastically reduced, and the profiles are in good agreement within ± 0.1 Mm^{-1} sr^{-1} (Figures 4b, 4f). ~~Note that the $\Delta\beta_{aer}$ discrepancy associated with the altitude displacement on 12 July 2018 increases after the FOV correction (Figure 4b).~~In relative terms, this corresponds to deviations of less than 10 % of the observed signal in the PBL, which is comparable to the estimated statistical uncertainty associated with the remote sensing measurements alone (see Section 2.1).

As already noted in Section 3.2~~3~~ ~~(Figure 2d)~~, the effect of the FOV correction on the CHM15K comparison is smaller. In p~~P~~articular~~ly~~, ~~we observe that~~ for the case of 4 September 2018 (Figure 4g-h) the ~~FOV~~ correction leads to a slight improvement in agreement with COBALD (≈ 0.05 Mm^{-1} sr^{-1}), whereas on 12 July 2018 (Figure 4c-d) it slightly increases the discrepancy ~~with COBALD~~. Due to the empirical implementation of the FOV correction, with many assumptions and simplifications involved (e.g., single-mode size distribution, coarse parameterization in AE-space~~, etc.~~), it is to be expected that for individual sounding the magnitude of ~~our~~ the correction might be underestimating or overestimating the true effect of the different FOVs. ~~Nevertheless, the FOV correction systematically improves the statistical comparison between COBALD and both RALMO and CHM15K, as will be discussed in the next section (see Tables 2-3).~~. The uncertainty introduced by the FOV correction in the statistical comparison will be discussed more in detail in Section 4.3.

4.2. Statistical comparison

Here we ~~discuss~~ present the results of the statistical comparison for the dataset introduced in Section 2.3, consisting of 17 simultaneous RALMO vs. COBALD profiles (Section 4.2.1) and 31 CHM15K vs. COBALD profiles (Section 4.2.2).

4.2.1. RALMO vs. COBALD

Figure 5 shows all data points of the RALMO – COBALD difference ($\Delta\beta_{aer}$ at 455 nm) as function of altitude, both expressed in absolute backscatter coefficient units (Panel a) and in percent units relative to the COBALD signal (Panel b), after the FOV correction was applied to all COBALD measurements. Medium-h~~H~~igh and ~~Low~~ low aerosol content measurements, classified as in Section 3.3, are shown by dark blue and light blue circles, respectively. The mean deviation (δ) and mean ± standard deviation ($\delta \pm \sigma$) ~~deviation~~ profiles of ~~Medium~~medium-~~High~~ high aerosol content data ~~data of $\Delta\beta_{aer}$~~ are shown in both panels

Formatiert: Schriftart: Kursiv

as ~~shown by~~ thick ~~solid~~ and thin solid ~~dashed~~ black lines, respectively~~, respectively~~. As discussed in Section 3~~.1~~, to avoid in-cloud measurements, we only consider data points with RH < 90% (according to the radiosonde measurements).

Medium-high aerosol content measurements of RALMO and COBALD β_{aer} ~~measurements a~~ are on average in good agreement over the entire altitude range (~~0.8~~ 0.8-6 km asl), yet significant discrepancies can occur in ~~single~~ individual profiles~~, and the standard deviation is not constant with altitude~~. As expected, the largest absolute differences are observed ~~For z > 2.5 km, typically corresponding to the free troposphere (i.e. above the PBL), the absolute differences between RALMO and COBALD are small (Figure 5a), while their relative differences are large (Figure 5b). This is mostly due to the low aerosol content, hence the low absolute backscattered signal, in 'clean' free-tropospheric air masses. The absolute $\Delta\beta_{aer}$ differences for z > 2.5 km are smaller than 0.1 Mm⁻¹ sr⁻¹ for the majority of data points (Figure 5a), yet their relative discrepancies often exceed ± 100% of the signal, and the mean $\Delta\beta_{aer}$ profile varies between 0-30 % (Figure 5b).~~

~~F~~at low altitudes (z <~~or~~ 3~~z < 2.5~~ km), ~~which approximately corresponds to the average top of~~ including most of the PBL (hence ~~PBL altitude~~ medium-high aerosol content) measurements in our dataset (Figure 5a). Conversely~~in our dataset~~, smaller absolute discrepancies, yet large relative differences (Figure 5b), are found in the free troposphere (z > 3 km), where low aerosol content measurements prevail.

For z < ~~2.5~~3 km, ~~the discrepancies between RALMO and COBALD are larger in absolute terms (Figure 5a), but smaller in relative terms (Figure 5b) compared to the free troposphere.~~ the mean ~~$\Delta\beta_{aer}$~~ deviation profile (δ) of ~~Medium-High~~medium-high aerosol content data stays within ± 0.1 Mm^{-1} sr^{-1}~~, with~~ while standard deviation (σ) ~~≈~~ ranges between 0.1-0.4~~25~~ Mm^{-1} sr^{-1}, ~~while~~ and individual data points rarely exceed ± 0.5 Mm^{-1} sr^{-1} (Figure 5a). In relative terms, δ shows an average slight overestimation of 5-10~~-10~~ % below 2 km (with σ ≈ ~~≈ 40~~40 %), and an underestimation of 10-25 % between 2-3 km (σ ≈ ~~≈ 40~~30 %) (Figure 5b). ~~A large fraction of this high variability can be attributed to the atmospheric variability effects discussed in Section 3.1Such a~~Such ~~relatively~~ large relative standard deviations can be at least partly attributed to~~, discussed in see Figures 3-4, S3-S4~~2 the uncertainties associated with the wavelength conversion and FOV correction of the data (Sections 3.1-3.2) and spatial and temporal variability effects (Section 2.4). The~~i~~se issues ~~issue~~ will be discussed ~~more~~ in more detail in Section ~~5~~4.3.

For z > ~~2.5~~3 km~~,~~ , ~~typically corresponding to the free troposphere (i.e. above the PBL), the absolute differences between RALMO and COBALD are small (Figure 5a), while their relative differences are large (Figure 5b). This is mostly due to the low aerosol content, hence the low absolute backscattered signal, in 'clean' free-tropospheric air masses. The~~nearly all ~~the observed~~absolute ~~absolute $\Delta\beta_{aer}$~~ differences ~~for z > 2.5 km~~ are smaller than ± 0.1 Mm^{-1} sr^{-1} ~~for the majority of data points~~ (Figure 5a)~~, yet their relative discrepancies often exceed ± 100% of the signal, and the mean $\Delta\beta_{aer}$ profile varies between 0-30 % (Figure 5b).~~ ~~Medium-High~~Medium-high aerosol content data points above 3 km altitude ~~are~~ generally ~~mostly found~~stay within ~~a~~ deviations of ± 50 % ~~discrepancy~~, whereas low aerosol content ones often exceed ± 100 % (Figure 5b).

~~To quantify the spread of $\Delta\beta_{aer}$,~~ Figure 6 shows the frequency of occurrence distribution of ~~the~~ RALMO – COBALD $\Delta\beta_{aer}$~~, difference,~~ calculated for the altitude intervals of 0.8-3~~0 – 2~~ km (Panels ~~e-f~~a-b), ~~, 2-4~~3-6~~ –~~ km (Panels c-d) and ~~800 m – 6~~0.8-

Formatiert: Schriftart: Nicht Kursiv

Formatiert: Schriftart: Nicht Kursiv

Formatiert: Schriftart: Kursiv

Formatiert: Schriftart: Nicht Kursiv

Formatiert: Schriftart: Kursiv

6 km (i.e., all altitudes~~,~~: Panels e-f), ~~4-6 km (Panels a-b) (note that the first interval only contains data from above 800 m asl, as discussed in Section 3.1~~for medium-high aerosol content data (blue bars) and all data (i.e., including low aerosol content: black lines). The distributions are calculated both in absolute units, within 40 intervals of 0.1 Mm^{-1} sr^{-1} width between ±2 Mm^{-1} sr^{-1} (~~left column plots~~Panels a, c, e), and in relative units within 40 intervals of 10 % width between ±200 % (Panels b, d, f~~right column~~). ~~Note that the values of The mean values and standard deviations of each distribution are given in Table 2.~~

In all distributions, medium-high aerosol content measurements show a higher frequency of occurrence of small relative deviations compared to all data (Figure 6b, 6d, 6f), and a lower frequency of occurrence of small absolute differences (Figure 6b, 6d, 6f). The absolute (relative) $\delta \pm \sigma$ for medium-high aerosol content data are – 0.018 ± 0.237 Mm^{-1} sr^{-1} (– 2 % ± 37 %) for altitudes 0.8-3 km, + 0.015 ± 0.068 Mm^{-1} sr^{-1} (+ 13 % ± 38 %) for 3-6 km, and + 0.001 ± 0.141 Mm^{-1} sr^{-1} (+ 6 % ± 38 %) for all altitudes (see Table 2). Considering all data, $\delta \pm \sigma$ increases to +5 % ± 40 % for 0.8-3 km, + 19 % ± 53 % for 3-6 km, and + 13 % ± 47 % for all altitudes.

We observe that the skewedness of the medium-high aerosol content distribution for 0.8-3 km (Figure 6a-b) is strongly influenced by a single strongly outlying profile, showing $\Delta\beta_{aer}$ > 100 % at z < 2 km (see Figure 5b), which is likely related to atmospheric variability effects (see discussion in Section 4.3). ~~The frequency of occurrence distributions for z > 2 km highlight the small variability in absolute units (Figure 6a, 6c) and large variability in relative units (Figure 6b, 6d) already observed in Figure 5. The absolute standard deviation for 2-6 km altitude is around 0.12 Mm^{-1} sr^{-1} (Figure 6a, 6c), corresponding to up to 95 % of the signal, at 4-6 km (Figure 6b, 6d). For z < 2 km, the average RALMO – COBALD difference is +0.005 Mm^{-1} sr^{-1} (standard deviation 0.319 Mm^{-1} sr^{-1}) in absolute units (Figure 6e), and +6 % (standard deviation 40 %) in relative units (Figure 6f). The skewedness of the distributions towards large values is mainly due to a single outlying profile, showing discrepancies larger than +100 % at z < 2 km (see Figure 5b).~~

Finally, to evaluate their correlation, Figure 7 shows a ~~correlation~~ scatter ~~(scatter)~~ plot of all ~~COBALD~~ RALMO vs. ~~RALMO~~ COBALD measurements of β_{aer} at 455 nm (between 0.03-5 Mm^{-1} sr^{-1} ~~(Panel a), and two additional frequency of occurrence distributions of $\Delta\beta_{aer}$ (Panels b-c).~~). As in Figure 5, medium-high aerosol content data are shown as dark blue circles, and low aerosol content data as light blue circles. ~~The scatter plot includes all data points between altitudes 0.8-6 km of the 17 profiles considered for the comparison (blue circles) plus their mean correlation line (thick black line), calculated as the average β_{aer} from RALMO for each 0.2 Mm^{-1} sr^{-1} interval of β_{aer} from COBALD (Figure 7a).~~ Isolines of ~~1~~ $\Delta\beta_{aer}$ = 0~~:1 agreement~~, $\Delta\beta_{aer}$ = ±25 % and $\Delta\beta_{aer}$ = ±50 % differences are ~~also indicated~~indicated by ~~thin~~ solid, dashed and dotted black lines, respectively~~.~~ ~~The frequency of occurrence distributions, expressed both in absolute (Panel b) and relative units (Panel c), are calculated from all data points with COBALD β_{aer} > 0.2 Mm^{-1} sr^{-1}. This threshold is set to exclude all free tropospheric samples with negligible aerosol content, which may introduce large relative discrepancies despite of very small absolute differences (see bottom-left corner of Figure 7a)~~. The 0.1 Mm^{-1} sr^{-1} threshold in COBALD β_{aer} at 455 nm, separating low from medium-high aerosol content layers as described Section 3.3, is also shown as a thin vertical dashed line.

Figure 7~~a reveals~~ shows a good correlation between~~that the majority of~~ RALMO and COBALD measurements ~~measurements with~~in medium-high aerosol content conditions~~,~~ and~~β_{aer} > 0.2 Mm^{-1} sr^{-1} (at all altitudes) lie between a ± 25 % difference with~~

Formatiert: Schriftart: Nicht Kursiv

Formatiert: Schriftart: Nicht Kursiv

Formatiert: Schriftart: Kursiv

Formatiert: Schriftart: Kursiv

Formatiert: Nicht Hochgestellt/ Tiefgestellt

Formatiert: Schriftart: Nicht Kursiv

~~respect to COBALD, whereas~~ as expected, a larger spread for low aerosol content data ~~β_{aer} < 0.2 Mm^{-1} sr^{-1} deviations exceeding ± 100 % are commonly observed~~. The Pearson correlation coefficient (ρ) of from medium-high aerosol content data is + 0.81 for altitudes 0.8-3 km, + 0.62 for 3-6 km, and + 0.80 for all altitudes (see Table 2), indicating a high degree of linear correlation between RALMO and COBALD measurements up to 6 km. We note from Figure 7, that the highest density of medium-high aerosol content measurements is found at $\beta_{aer} \approx$ 0.4-2 Mm^{-1} sr^{-1}, suggesting that this interval represents the average PBL aerosol content in our dataset. Here, RALMO and COBALD show a particularly good agreement, with most individual differences staying below ± 25 % (Figure 7). ~~The average correlation line stays within ± 25 % for nearly the entire considered signal range, and approaches a 1:1 agreement between 0.6-1.4 Mm^{-1} sr^{-1} (Figure 7a), which is typically the relevant range of β_{aer} at 455 nm in the PBL (e.g., Figures 4, S4). Considering all data points with β_{aer} > 0.2 Mm^{-1} sr^{-1}, the average RALMO – COBALD difference is – 0.011 Mm^{-1} sr^{-1} (+ 1.7 %) with standard deviation 0.329 Mm^{-1} sr^{-1} (56 %) in absolute (relative) units, respectively (Figure 7b-c).~~

Formatiert: Schriftart: Kursiv

~~To summarize the statistical comparison, Table 2 reports mean values and standard deviations of RALMO – COBALD $\Delta\beta_{aer}$ for the three altitude intervals defined in Figure 6 (i.e., 2 km intervals between 0-6 km), and for the ensemble of all measurements with COBALD β_{aer} > 0.2 Mm^{-1} sr^{-1} as defined in Figure 7b-c. In addition to Figures 6-7, Table 2 shows the same results calculated both before and after the application of the FOV correction, which enables to evaluate its effect on the statistical comparison. The mean $\Delta\beta_{aer}$ decreases from 29 % to 6 % after the FOV correction for z < 2 km, and from 26 % to 2 % when considering all measurements with β_{aer} > 0.2 Mm^{-1} sr^{-1}. Above 2 km, the effect of the FOV correction is smaller (e.g., 33 % to 29 % at 4-6 km) due to the prevalence of free tropospheric air masses (with high AE) that are unaffected by the correction (see Figure 2d). The standard deviations are weakly affected by the FOV correction (e.g., 45 % to 40 % for z < 2 km).~~

4.2.2. CHM15K vs. COBALD

Following the same structure of the previous subsection, here we analyze the CHM15K vs. COBALD statistical comparison first in terms of vertical profiles (Figure 8), then frequency of occurrence distributions (Figure 9), and finally scatter plot of all CHM15K vs. COBALD measurements (Figure 10).

Figure 8 shows all data points of $\Delta\beta_{aer}$ at 940 nm for CHM15K – COBALD as function of altitude, both in absolute backscatter coefficient units (Panel a) and percent units relative to the COBALD signal (Panel b). ~~Like in~~Analogously to Figure 5, medium-high aerosol content data are shown as dark red circles, and low aerosol content as orange circles~~the FOV correction is applied to all COBALD measurements, and only data points with RH < 90 % are considered~~. Note that the higher density of data points in Figure 8 compared to Figure 5 is due to the larger number of profiles considered for the CHM15K vs. COBALD comparison (31) relative to the RALMO vs. COBALD comparison (17) (see Section 2.3).

In absolute ~~units~~terms, ~~the~~ medium-high aerosol content ~~CHM15K~~ measurements by CHM15K are on average in good agreement with COBALD over the entire altitude range (Figure 8a), ~~although~~ yet their relative differences are characterized by a

~~strong~~ large statistical ~~fluctuations~~ variability ~~at high altitudes~~at all altitudes (Figure 8b). The absolute differences in β_{aer} between CHM15K and COBALD are typically larger than observed for RALMO (Figure 5a), despite β_{aer} is smaller at 940 nm than at 455 nm due to its spectral dependency. This highlights the lower signal-to-noise ratio of CHM15K compared to a high-power Raman lidar as such RALMO, which results in the large relative fluctuations of $\Delta\beta_{aer}$ in the free troposphere in Figure 8b (especially for low aerosol content conditions).~~. For z > 2.5 km, the absolute differences between CHM15K and COBALD are smaller than ± 0.2 Mm^{-1} sr^{-1} for the majority of data points (Figure 8a), while the corresponding relative discrepancies often exceed ±100 % (Figure 8b). This is due to the low absolute backscattered signal and the low signal-to-noise ratio of CHM15K in the free troposphere. We observe that the absolute differences between CHM15K and COBALD (Figure 8a) are typically larger than for RALMO (Figure 5a) at all altitudes, despite β_{aer} is smaller at 940 nm than at 455 nm due to its spectral dependency. This highlights the lower signal-to-noise ratio of the CHM15K ceilometer compared to a high-power Raman lidar such as RALMO, and causes the large relative fluctuations of $\Delta\beta_{aer}$ in the free troposphere observed in Figure 8b.~~

Below 3 km altitude, ~~For z < 2.5 km, CHM15K~~the mean deviation profile of medium-high aerosol content measurements shows ~~on average~~ a slight overestimation of + 5% with respect to COBALD~~with respect to COBALD measurements~~, and a standard deviation of around 40% (Figure 8b). ~~. The mean $\Delta\beta_{aer}$ in the PBL is about +0.04 Mm^{-1} sr^{-1} with standard deviation 0.2 Mm^{-1} sr^{-1} (Figure 8a), corresponding to about +15 % (standard deviation ≈ 50 %) of the COBALD signal (Figure 8b). T~~In this case, such a~~he~~ ~~large standard deviation~~large spread of relative deviations can be also partly ~~again partly~~ attributed (in addition the effects mentioned in Section 4.2.1) to the uncertainty ~~atmospheric variability effects, in addition to the lower signal-to-noise ratio of CHM15K discussed above. The slight positive bias of CHM15K with respect to COBALD for z < 2.5 km could be due to minor unsolved geometric overlap issues in the ceilometer's retrieval algorithm, or (more likely)~~ related ~~to~~ with the assumption of a constant lidar ratio (50 sr) for all profiles, made in the Klett inversion scheme for the retrieval of the CHM15K backscatter coefficient~~, used for the retrieval of β_{aer} from CHM15K~~ (see Section 2.1). This uncertainty will be discussed in more detail in Section 4.3. For z > ~~2.5~~3 km, the ~~absolute differences between CHM15K and COBALD are smaller~~majority of medium-high aerosol content measurements (except one outlying profile, showing discrepancies of up to − 0.5 Mm^{-1} sr^{-1} until 4 km altitude) stay within absolute deviations of ~~than~~ ± 0.2 Mm^{-1} sr^{-1} (Figure 8a) ~~for the majority of data points (Figure 8a), while the corresponding relative discrepancies~~. ~~often exceed ±100 % (Figure 8b). This is due to the low absolute backscattered signal and the low signal-to-noise ratio of CHM15K in the free troposphere.~~

~~We observe that the absolute differences between CHM15K and COBALD (Figure 8a) are typically larger than for RALMO (Figure 5a) at all altitudes, despite β_{aer} is smaller at 940 nm than at 455 nm due to its spectral dependency. This highlights the lower signal-to-noise ratio of the CHM15K ceilometer compared to a high-power Raman lidar such as RALMO, and causes the large relative fluctuations of $\Delta\beta_{aer}$ in the free troposphere observed in Figure 8b.~~

Figure 9 shows ~~the~~ frequency of occurrence distributions of CHM15K – COBALD $\Delta\beta_{aer}$ at 940 nm ~~for the altitude intervals of~~ for the altitude intervals of 0.8-3 km (Panels a-b), 3-6 km (Panels c-d) and 0.8-6 km (i.e. all altitudes: Panels e-f), both for medium-high aerosol content data (red bars) and all data (black solid lines), calculated as in Figure 6. The absolute (relative) $\delta \pm \sigma$ for medium-high aerosol content data are + 0.009 ± 0.185 Mm^{-1} sr^{-1} (+ 5 % ± 43 %) for 0.8-3 km altitudes, − 0.081 ± 0.291 Mm^{-1} sr^{-1} (− 43 % ± 72 %) for 3-6 km, and − 0.058 ± 0.205 Mm^{-1} sr^{-1} (− 22 % ± 59 %) for all altitudes. Similarly to as for RALMO, including low aerosol content data increases the frequency of occurrence of small absolute differences (Figure 9a, 9c, 9e), yet reduces the frequency of occurrence of small relative differences (Figure 9b, 9d, 9f). In particular for z > 3 km, we observe that the distributions of relative $\Delta\beta_{aer}$ for all data are significantly broader for CHM15K (Figure 9d) than for RALMO (Figure 6d). This again denotes the lower signal-to-noise ratio of CHM15K with respect to RALMO at high altitudes. ~~0-2 km (Panels e-f), 2-4 km (Panels c-d), and 4-6 km (Panels a-b), expressed both in absolute units (left column) and in percent units relative to the COBALD signal (right column), and calculated as in Figure 6. The frequency of occurrence distributions for z > 2 km again highlight the small variability of $\Delta\beta_{aer}$ in absolute units (Figure 9a, 9c) and large variability in relative units (Figure 9b, 9d) in the free troposphere. We observe that the spread of the $\Delta\beta_{aer}$ distributions, and particularly the associated standard deviations, are larger for CHM15K (e.g., 320 % at 2-4 km, Figure 9d; 640% at 4-6 km, Figure 9b) than for RALMO (see Figure 6). For z < 2 km (Figure 9e-f), the mean CHM15K – COBALD difference is + 0.038 Mm^{-1} sr^{-1} (+13 %) with standard deviation 0.207 Mm^{-1} sr^{-1} (51 %) in absolute (relative) units, respectively.~~

~~Finally~~Finally, ~~, analogously to Figure 7,~~ Figure 10 shows the scatter plot of all CHM15K vs. COBALD measurements of β_{aer} at 940 nm (between 0.01-3 Mm^{-1} sr^{-1}). As in Figure 8, medium-high aerosol content data points are shown as dark red circles, and low aerosol content as orange circles. The 0.05 Mm^{-1} sr^{-1} threshold in COBALD β_{aer}, separating low from medium-high aerosol content data at 940 nm (as described in Section 3.3), is shown by a thin black dashed line. CHM15K and COBALD show a generally good correlation in the medium-high aerosol content range, although discrepancies exceeding ± 50 % are often observed, and a very large spread of deviations for low aerosol content data (Figure 10). The Pearson correlation coefficient is ρ = + 0.72 for altitudes 0.8 -3 km asl, + 0.24 for altitudes 3-6 km asl, and + 0.62 for all altitudes, indicating a generally high degree of correlation at low altitudes (yet with smaller ρ than for RALMO), and a lower correlation as high altitudes. We observe that in the range of most frequently observed β_{aer} in the PBL (approximately 0.2-1 Mm^{-1} sr^{-1}), CHM15K regularly exceeds deviations of ± 25 % with respect to COBALD (Figure 10), while for RALMO in corresponding range of β_{aer} (0.4-2 Mm^{-1} sr^{-1} at 455 nm), the fraction of individual differences exceeding ± 25 % in significantly smaller (Figure 7). This highlight a generally better precision of RALMO with respect to CHM15K, even at medium-high aerosol content conditions.

4.3. Discussion

The results of the statistical comparison for medium-high aerosol content data are summarized in Tables 2-3. In general, both RALMO and CHM15K achieve a good agreement with COBALD in terms of mean deviations in the PBL (δ = − 2 % for RALMO and + 5 % for CHM15K, for z < 3 km), while simultaneously they show relatively large standard deviations, even at

Formatiert: Schriftart: Kursiv

Formatiert: Schriftart: Kursiv

Formatiert: Schriftart: Kursiv

low altitudes (σ = 37 % for RALMO, 43 % for CHM15K, z < 3 km). As mentioned throughout the paper, this can be at least partly attributed to a number of methodological and technical aspects of our comparison, namely, the uncertainties associated with the wavelength conversion and the FOV correction, and spatial and temporal variability effects.

The first uncertainty is related to the assumption of the COBALD-derived AE profiles to perform the wavelength conversion of the lidar data. From Equation 2 we can derive that an error of 0.2 in AE, which is a conservative estimate considering the small difference between the wavelengths that are compared, results in an error of 5 % in β_{aer} for the 355-to-455 nm conversion, and 2.5 % for the 1064-to-940 nm conversion. The second factor is related to the empirical implementation of the FOV correction, which involves several assumptions and simplifications (see Section 3.3). From Figure 2b, we can estimate an uncertainty of up to ± 20% in β_{aer} for the PBL (for both 455 and 940 nm), due to variability of the correction factors in the range of AE = 0.8-1.5, which is not resolved by the parameterization of the FOV correction factors in AE-space (Figure 2d). Finally, the balloon's horizontal drift with altitude away from the lidar beam, and the different integration times of the two techniques, can also affect the spread of their measurements. These effects can lead to large discrepancies over small altitude layers, as in the case of strong vertical gradients in β_{aer} (e.g., top of boundary layer: Figure 4a-d), as well as potentially over larger altitude regions, due to the horizontal gradient of the β_{aer} field around the station (e.g., in the case of the strongly outlying profiles of the statistical comparison: see Figures 5, 8). The lack of information on the aerosol size distribution, and the high spatial and temporal variability of atmospheric aerosols, prevent an accurate quantification of these artifacts, which inevitably affect the standard deviations of our statistical comparison.

In addition to these effects, the large spread of relative deviations below 3 km in the case of CHM15K − COBALD can be also related to the assumption of a constant lidar ratio (50 sr) for all profiles, made in the Klett retrieval algorithm (see Section 2.1). Using a similar ceilometer (Jenoptik CHM15kx), Wiegner and Geiss (2012) estimate that an error of ± 10 sr in lidar ratio leads to an error in β_{aer} smaller than 2 % in the boundary layer. Ackermann (1998) shows that 50 ± 10 sr represents well the expected range of variability of the lidar ratio of continental aerosol in the infrared spectrum, for all RH conditions between 0-90 %. Therefore, this uncertainty conceivably plays a minor role compared to the effects discussed above.

Despite of these limitations, the comparison of individual profiles (Section 4.1) shows that both RALMO and CHM15K are able to achieve an excellent agreement with COBALD measurements, including the correct representation of fine and complex structures in the β_{aer} vertical profiles (Figures 3-4, S2-S3). In particular, the case study of 12 July 2018 (Figures 4a-d) shows differences between the lidars and COBALD which are smaller than expected statistical uncertainty associated with the remote sensing measurements alone (10-15 %, see Section 2.1). This suggests that, under optimal conditions (such as, no wind shear, uniform β_{aer} field, mono-modal aerosol size distribution), the deviations between the two lidars and COBALD are typically smaller than the average σ of our statistical comparison. Considering also the good linear correlation achieved by both lidars (ρ = + 0.81 for RALMO, + 0.72 for CHM15K, for z < 3 km), we conclude that β_{aer} measurements by RALMO and CHM15K are in overall good agreement with in-situ measurements by COBALD sondes up to 6 km altitude.

~~shows a scatter plot of all COBALD vs. CHM15K measurements of β_{aer} at 940 nm (Panel a), plus two additional frequency of occurrence distributions of $\Delta\beta_{aer}$ (Panels b-c). The scatter plot includes all data points between altitudes 0.8-6 km of the 31~~

Formatiert: Schriftart: Nicht Kursiv

Formatiert: Schriftfarbe: Text 1

Formatiert: Schriftfarbe: Text 1

Formatiert: Schriftfarbe: Text 1

Formatiert: Schriftfarbe: Text 1

Formatiert: Schriftfarbe: Text 1, Nicht Hervorheben

Formatiert: Schriftfarbe: Text 1, Nicht Hervorheben

Formatiert: Schriftfarbe: Text 1

Formatiert: Schriftfarbe: Text 1

Formatiert: Schriftfarbe: Text 1

Formatiert: Schriftart: Kursiv, Schriftfarbe: Text 1

Formatiert: Schriftfarbe: Text 1

Formatiert: Schriftfarbe: Text 1

Formatiert: Schriftfarbe: Text 1

Formatiert: Schriftfarbe: Text 1

Formatiert: Schriftfarbe: Text 1

Formatiert: Schriftfarbe: Text 1

Formatiert: Schriftfarbe: Text 1

Formatiert: Schriftfarbe: Text 1

~~profiles considered for the comparison (orange circles), plus the mean COBALD vs. CHM15K correlation profile (thick black line), calculated as in Figure 7. The frequency of occurrence distributions, both in absolute (Panel b) and relative units (Panel c), are calculated from all data points with β_{aer} > 0.1 Mm^{-1} sr^{-1} (lowered threshold in order to account for the smaller values of β_{aer} at 940 nm compared to 455 nm).~~

~~Figure 10a shows a general overestimation of CHM15K compared to COBALD measurements in the range of approximately 0.4-1.2 Mm^{-1} sr^{-1}, which is consistent with the vertical profiles shown in Figure 8. Most of the data points in this interval are found in the top-left quadrant of the scatter plot, with discrepancies often exceeding +50 % of the COBALD signal, while their mean correlation line stays between 0-25 % (Figure 10a). When all measurements with β_{aer} > 0.1 Mm^{-1} sr^{-1} are considered, the average CHM15K – COBALD difference is – 0.001 Mm^{-1} sr^{-1} (+1.9 %) with standard deviation of 0.281 Mm^{-1} sr^{-1} (43 %) in absolute (relative) units, respectively (Figure 10b-c).~~

~~In summary, Table 3 shows mean values and standard deviations of CHM15K – COBALD $\Delta\beta_{aer}$ for the three altitude intervals defined in Figure 9, and for the ensemble of all measurements with COBALD β_{aer} > 0.1 Mm^{-1} sr^{-1} defined in Figure 10b-c. As in Table 2, here we show the same results both as calculated before and after the application of the FOV correction. The mean CHM15K – COBALD $\Delta\beta_{aer}$ decreases due to the FOV correction from 25% to 13% for z < 2 km, and from 16 % to 2% when considering all measurements with β_{aer} > 0.1 Mm^{-1} sr^{-1}. For z > 2 km, the effect of the correction is small.~~

5. Conclusions

We have presented the first comparison of lower tropospheric aerosol backscatter coefficient (β_{aer}) profiles retrieved by remote sensing instruments against independent in-situ measurements. The two analyzed lidar systems, one research Raman lidar (RALMO) and one commercial ceilometer (CHM15K), were validated using simultaneous and co-located balloon soundings carrying a Compact Backscatter Aerosol Detector (COBALD), performed during the years 2014-2019 at the MeteoSwiss observatory of Payerne, Switzerland. COBALD provides high-precision in-situ measurements of β_{aer} at two wavelengths (455 and 940 nm) and is used as the reference instrument. The β_{aer} profiles retrieved from RALMO (355 nm) and CHM15K (1064 nm) are converted to respectively 455 nm and 940 nm using the altitude-dependent Angstrom exponent (AE) profiles retrieved from COBALD data. To account for the different receiver field of view (FOV) angles between the remote sensing instruments (0.01-0.02°) and COBALD (6°), we derived a FOV correction using Mie-theory scattering simulations. The correction factors are parametrized as functions of AE to account for the size-dependency of the solutions. For the statistical comparison, low and medium-high aerosol content measurements are separated according to an empirical threshold in β_{aer}.

The comparison of individual profiles shows that both RALMO and CHM15K achieve a good agreement with COBALD β_{aer} measurements in the boundary layer and free troposphere, up to 6 km altitude, including fine structures in the aerosol's vertical distribution. The mean ± standard deviation of RALMO – COBALD $\Delta\beta_{aer}$ (at 455 nm) for medium-high aerosol content data is – 0.018 ± 0.237 Mm^{-1} sr^{-1} (– 2 % ± 37 %) for altitudes 0.8-3 km asl, and + 0.001 ± 0.141 Mm^{-1} sr^{-1} (+ 6 % ± 38 %) for all

Formatiert: Schriftart: Kursiv

altitudes between 0.8-6 km asl. For CHM15K – COBALD, the mean ± standard deviation of $\Delta\beta_{aer}$ (at 940 nm) for medium-high aerosol measurements is + 0.009 ± 0.185 Mm^{-1} sr^{-1} (+ 5 % ± 43 %) for altitudes 0.8-3 km, and − 0.058 ± 0.205 Mm^{-1} sr^{-1} (− 22 % ± 59 %) for all altitudes. The Pearson correlation coefficient for medium-high aerosol content below 3 km altitude is data is + 0.81 for RALMO vs. COBALD and + 0.72 for CHM15K vs. COBALD, indicating a high degree of linear correlation between both lidars and the in-situ measurements. For altitudes above 3 km (i.e., in the free troposphere), absolute deviations generally decrease while relative deviations increase, due to the prevalence of low aerosol content air masses. The standard deviations of medium-high aerosol content data between 3-6 km altitude are 38 % (0.068 Mm^{-1} sr^{-1}) for RALMO – COBALD and 59 % (0.205 Mm^{-1} sr^{-1}) for CHM15K – COBALD, which denotes the lower signal-to-noise ratio of CHM15K compared to a high-power Raman lidar system such as RALMO.

While both RALMO and CHM15K agree well with COBALD in terms of mean deviations, the statistical comparison is characterized by relatively large standard deviations for both instruments at all altitudes. As discussed in Section 4.3, this can be at least partly attributed to a number of technical aspects of our comparison, most notably the uncertainty associated with the FOV correction and spatial and temporal variability effects (related with the balloon's horizontal drift with altitude and different integrations times), which contribute to the spread of the measurements. Due to the lack of information on the aerosol size distribution and the high spatial and temporal variability of atmospheric aerosols, these effects cannot be accurately quantified. Nevertheless, the excellent agreement observed in individual profiles, including fine and complex structures in the aerosol's vertical distribution, shows that under optimal conditions (no wind shear, uniform β_{aer} field, mono-modal aerosol size distribution), the deviations between the two lidars and COBALD are typically comparable to the estimated statistical errors of the remote sensing measurements alone (10-15 %). Similar or even larger discrepancies are also reported in the literature between single-wavelength elastic backscatter and Raman lidars (e.g., Matthais et al., 2004), as well as between different Raman lidar algorithms (Pappalardo et al., 2004).

~~For altitudes below 2 km, the mean ± standard deviation difference in β_{aer} obtained from the statistical comparison of all available profiles is +6 ± 40 % (+0.005 ± 0.319 Mm^{-1} sr^{-1}) for RALMO – COBALD at 455 nm, and +13 ± 51 % (+0.038 ± 0.207 Mm^{-1} sr^{-1}) for CHM15K – COBALD at 940 nm. The high standard deviations can be largely attributed to atmospheric variability effects related to fundamentally different characteristics of the remote sensing and balloon sounding techniques, as the balloon's horizontal drift with altitude (away from the lidar beam) and the different integration times. Combined with the high spatial and temporal variability of atmospheric aerosols, these effects often result into the smearing and/or slight altitude displacement of aerosol backscatter features that are seen by both techniques (see Figures 3-4, S3-S4).largely:parameterization in ThisdeviationsFigure 4a-d (e.g., in the case of the strongly outlying profile in Figure 5b),,stronglystatistical comparisonthe absence of a statistically significant bias(t)andexcellent (below the statistical uncertainty of the lidar measuremens)profilesshow the average of our~~

~~As mentioned in Section 4.2.1, the standard deviation of RALMO – COBALD in the boundary layer is strongly influenced by one single outlying profile in our dataset (see Figure 5b). For this reason, it is interesting to note that the interquartile range of the RALMO – COBALD distribution for z < 2 km ranges between -20 % and +8 %, and for CHM15K – COBALD between~~

Formatiert: Schriftart: Nicht Kursiv

Formatiert: Schriftfarbe: Text 1

Formatiert: Schriftfarbe: Text 1

Formatiert: Schriftfarbe: Text 1

Formatiert: Schriftfarbe: Text 1

~~-22 % and +27 % (see Figures 6f-7f). This highlights the better precision of RALMO measurements with respect to CHM15K in the boundary layer. The slightly higher mean discrepancy between CHM15K and COBALD (+13 %) compared to RALMO (+6 %) could be either due to minor unsolved geometric overlap issues in the ceilometer's retrieval algorithm, or related to the assumption of a constant lidar ratio for all profiles (50 sr) made in the Klett inversion scheme.~~

~~For altitudes between 2-6 km, the standard deviations of both RALMO and CHM15K decrease in absolute terms (below 0.13 Mm^{-1} sr^{-1} and 0.16 Mm^{-1} sr^{-1}, respectively), while they increase in relative terms (often exceeding 100% of the signal). This is due to the low aerosol content (hence low absolute backscattered signal) in the free troposphere, and the vertically decreasing signal-to-noise ratio of the lidar instruments (especially CHM15K).~~

Considering the many uncertainties that characterize the retrieval of aerosol backscatter profiles from lidar instruments, from technical and instrumental effects to issues related with the mathematical treatment of the data (e.g., Pappalardo et al., 2004), our validation using fully independent in-situ measurements is particularly valuable. ~~Our~~ Despite of the limitations outlined above, results demonstrate that both single-wavelength (ceilometer) and Raman lidars can provide altitude-resolved measurements that are quantitatively consistent with high-precision balloon-borne measurements, over the ~~boundary layer~~PBL and free troposphere altitude regions. ~~In particular, net of atmospheric variability effects, it is interesting to observe that the discrepancies observed here are comparable to those previously found between ceilometer and Raman lidars (Matthais et al., 2004) and between different Raman lidar processing algorithms (Pappalardo et al., 2004).~~ ~~Hence~~Overall, we conclude that aerosol backscatter coefficient measurements by the RALMO and CHM15K lidar systems are in satisfactory agreement with in-situ measurements by COBALD sondes up to 6 km altitude.

References

Ackermann, J.,: The extinction-to-backscatter ratio of tropospheric aerosol: A numerical study, J. of Atmospheric and Oceanic Technology, 15, 1043-1050, 1998.

Amiridis, V., Balis, D. S., Kazadzis, S., Bais, A., Giannakaki, E., Papayannis, A., and Zerefos, C.: Four-year aerosol observations with a Raman lidar at Thessaloniki, Greece, in the framework of European Aerosol Research Lidar Network (EARLINET), J. Geophys. Res., 110, D21203, DOI: 10.1029/2005JD006190, 2005.

Ansmann, A., Riebesell, M., and Weitkamp, C.:Measurement of atmospheric aerosol extinction profiles with a Raman lidar, Opt. Lett. 15, 746–748, 1990.

Ansmann, A., Wandinger, U., Riebesell, M., Weitkamp, C., and Michaelis, W.: Independent measurement of the extinction and backscatter profiles in cirrus clouds by using a combined Raman elastic-backscatter lidar, Appl. Opt. 31, 7113–7131, 1992.

Bindoff, N., Stott, P., AchutaRao, K., Allen, M., Gillett, N., Gutzler, D., Hansingo, K., Hegerl, G., Hu, Y., Jain, S., Mokhov, I., Overland, J., Perlwitz, J., Sebbari, R., and Zhang, X.: Detection and Attribution of Climate Change: from Global to Regional. In: Climate Change 2013: The Physical Science Basis. Contribution of Working Group I to the Fifth Assessment

Formatiert: Englisch (Vereinigte Staaten)

Report of the Intergovernmental Panel on Climate Change [Stocker, T.F., D. Qin, G.-K. Plattner, M. Tignor, S.K. Allen, J. Boschung, A. Nauels, Y. Xia, V. Bex and P.M. Midgley (eds.)], Cambridge University Press, Cambridge, United Kingdom and New York, NY, USA., pp. 867–952, 2013.

Bösenberg, J., Matthias, V., Linné, H., Comerón Tejero, A., Rocadenbosch Burillo, F., Pérez López, C., and Baldasano Recio, J. M.: EARLINET: A European Aerosol Research Lidar Network to establish an aerosol climatology, Report. Max-Planck-Institut fur Meteorologie, pp. 1–191, 2003.

Brabec, M., Wienhold, F. G., Luo, B. P., Vömel, H., Immler, F., Steiner, P., Hausammann, E., Weers, U. and Peter, T.: Particle backscatter and relative humidity measured across cirrus clouds and comparison with microphysical cirrus modelling, Atmos. Chem. Phys., 12, 9135-9148, doi:10.5194/acp-12-9135-2012, 2012.

Brocard, E., Philipona, R., Haefele, A., Romanens, G., Mueller, A., Ruffieux, D., Simeonov, V., and Calpini, B.: Raman Lidar for Meteorological Observations, RALMO – Part 2: Validation of water vapor measurements, Atmos. Meas. Tech., 6, 1347–1358, https://doi.org/10.5194/amt-6-1347-2013, 2013.

Brunamonti, S., Jorge, T., Oelsner, P., Hanumanthu, S., Singh, B. B., Kumar, K. R., Sonbawne, S., Meier, S., Singh, D., Wienhold, F. G., Luo, B. P., Boettcher, M., Poltera, Y., Jauhiainen, H., Kayastha, R., Karmacharya, J., Dirksen, R., Naja, M., Rex, M., Fadnavis, S., and Peter, T.: Balloon-borne measurements of temperature, water vapor, ozone and aerosol backscatter on the southern slopes of the Himalayas during StratoClim 2016–2017, Atmos. Chem. Phys., 18, 15937–15957, https://doi.org/10.5194/acp-18-15937-2018, 2018.

Bucholtz, A.: Rayleigh-scattering calculations for the terrestrial atmosphere, Appl. Optics, 34, 15, 1995.

Cirisian, A., Luo, B. P., Engel, I., Wienhold, F. G., Sprenger, M., Krieger, U. K., Weers, U., Romanens, G., Levrat, G., Jeannet, P., Ruffiex, D., Philipona, R., Calpini, B., Spichtinger, P. and Peter, T.: Balloon-borne measurements of milatitude cirrus clouds, Atmos. Chem. Phys., 14, 7341-7365, doi:10.5194/acp-14-7341-2014, 2014.

Collis, R. T. H., and Russell, P. B.: Lidar measurement of particles and gases by elastic backscattering and differential absorption, in Laser Monitoring of the Atmosphere, E. D. Hinkley, pp. 71–151, Ed. Springer-Verlag, Berlin, 1976.

Dinoev, T., Simeonov, V., Calpini, B., and Parlange, M. B.: Monitoring of Eyjafjallajökull ash layer evolution over Payerne Switzerland with a Raman lidar, Proceedings of the TECO, Helsinki, Finland, 2010

Dinoev, T., Simeonov, V., Arshinov, Y., Bobrovnikov, S., Ristori, P., Calpini, B., Parlange, M., and van den Bergh, H.: Raman Lidar for Meteorological Observations, RALMO – Part 1: Instrument description, Atmos. Meas. Tech., 6, 1329–1346, https://doi.org/10.5194/amt-6-1329-2013, 2013.

Engel, I., Luo, B. P., Khaykin, S. M., Wienhold, F. G., Vömel, H., Kivi, R., Hoyle, C. R., Gross, J.-U., Pitts, M. C., and Peter, T.: Arctic stratospheric dehydration - Part 2: Microphysical modeling, Atmos. Chem. Phys., 14, 3231-3246, doi:10.5194/acp-14-3231-2014, 2014.

Haywood, J. and Boucher, O.: Estimates of the direct and indirect radiative forcing due to tropospheric aerosols: A review, Rev. Geophys., 38, 513–543, 2000.

Hervo, M., Poltera, Y., and Haefele, A.: An empirical method to correct for temperature-dependent variations in the overlap function of CHM15k ceilometers, Atmos. Meas. Tech., 9, 2947–2959, https://doi.org/10.5194/amt-9-2947-2016, 2016

Hicks-Jalali, S., Sica, R. J., Haefele, A., and Martucci, G.: Calibration of a water vapour Raman lidar using GRUAN-certified radiosondes and a new trajectory method, Atmos. Meas. Tech., 12, 3699–3716, https://doi.org/10.5194/amt-12-3699-2019, 2019.

Hicks-Jalali, S., Sica, R. J., Haefele, A., Martucci, G., Maillard Barras, E., and Voirin, J.: A Raman Lidar Tropospheric Water Vapour Climatology and Height-Resolved Trend Analysis over Payerne Switzerland, Atmos. Chem. Phys. Discuss., https://doi.org/10.5194/acp-2019-1089, in review, 2020.

Khaykin, S., Pommereau, J.-P., Korshunov, L., Yushkov, V., Nielsen, J., Larsen, N., Christensen, T., Garnier, A., Lukyanov, A., and Williams, E.: Hydration of the lower stratosphere by ice crystal geysers over land convective systems, Atmos. Chem. Phys., 9, 2275–2287, https://doi.org/10.5194/acp-9-2275-2009, 2009.

Lufft: User Manual Lufft CHM 15K Ceilometer, https://www.lufft.com/fileadmin/lufft.com/07_downloads/1_manuals/Manual_CHM15k_EN_R14.pdf, 2019 (accessed 8 Junuary 2020).

Luo, B. P., Voigt, C., Fueglistaler, S., and Peter, T.: Extreme NAT supersaturations in mountain wave ice PSCs: A clue to NAT formation, J. Geophys. Res., 108(D15), 4441, doi:10.1029/2002JDX00000, 2003.

Martucci, G.,Voirin, J., Simeonov, V. ,Renaud ,L. ,and Haefele, A.: A novel automatic calibration system for water vapor Raman LIDAR, in: EPJ Web of Conferences, EDP Sciences, 176, 05008, https://doi.org/10.1051/epjconf/201817605008, 2018.

Matthais, V., Freudenthaler, V., Amodeo, A., Balin, I., Balis, D., Bösenberg, J., Chaikovsky, A., Chourdakis, G., Comeron, A., Delaval, A., De Tomasi, F., Eixmann, R., Hågård, A., Komguem, L., Kreipl, S., Matthey, R., Rizi, V., Rodrigues, J. A., Wandinger, U., and Wang, X.: Aerosol lidar intercomparison in the framework of the EARLINET project. 1. Instruments, Appl. Opt. 43, 4, 961-976, https://doi.org/10.1364/AO.43.000961, 2004.

MeteoLabor: SRS-C34 Digital Radiosonde Information Sheet, http://www.meteolabor.ch/fileadmin/user_upload/pdf/meteo/UpperAir/srs-c34_e.pdf, 2010 (accessed 8 January 2020).

Navas-Guzmán, F., Guerrero-Rascado, J. L., Alados-Arboledas, L.: Retrieval of the lidar overlap function using Raman signals, Óptica Pura y Aplicada, 44, 71-75, 2011.

Navas-Guzmán, F., Bravo-Aranda, J. A., Guerrero-Rascado, J. L., Granados-Muñoz, M. J., and Alados-Arboledas, L.: Statistical analysis of aerosol optical properties retrieved by Raman lidar over Southeastern Spain, Tellus B, 65, 21234, doi:10.3402/tellusb.v65i0.21234, 2013.

Navas-Guzmán, F., Martucci, G., Collaud Coen, M., Granados-Muñoz, M. J., Hervo, M., Sicard, M., and Haefele, A.: Characterization of aerosol hygroscopicity using Raman lidar measurements at the EARLINET station of Payerne, Atmos. Chem. Phys., 19, 11651–11668, https://doi.org/10.5194/acp-19-11651-2019, 2019.

Nyeki, S., Halios, C., Baum, W., Eleftheriadis, K., Flentje, H., Gröbner, J., Vuilleumier, L., and Wehrli, C.: Ground-based aerosol optical depth trends at three high-altitude sites in Switzerland and southern Germany from 1995 to 2010, J. Geophys. Res.-Atmos., 117, D18202, https://doi.org/10.1029/2012JD017493, 2012.
Pappalardo, G., Amodeo, A., Pandolfi, M., Wandinger, U., Ansmann, A., Bösenberg, J., Matthais, V., Amiridis, V., De Tomasi, F., Frioud, M., Iarlori, M., Komguem, L., Papayannis, A., Rocadenbosch, F., and Wang, X.: Aerosol lidar intercomparison in the framework of the EARLINET project. 3. Raman lidar algorithm for aerosol extinction, backscatter, and lidar ratio, Appl. Opt. 43, 28, 5370-5385, https://doi.org/10.1364/AO.43.005370, 2004.
Pappalardo, G., Amodeo, A., Apituley, A., Comeron, A., Freudenthaler, V., Linné, H., Ansmann, A., Bösenberg, J., D'Amico, G., Mattis, I., et al.: EARLINET: towards an advanced sustainable European aerosol lidar network, Atmospheric Measurement Techniques, pp. 2389–2409, 2014.
Poltera, Y., Martucci, G., Collaud Coen, M., Hervo, M., Emmenegger, L., Henne, S., Brunner, D., and Haefele, A.: PathfinderTURB: an automatic boundary layer algorithm. Development, validation and application to study the impact on in situ measurements at the Jungfraujoch, Atmos. Chem. Phys., 17, 10051–10070, https://doi.org/10.5194/acp-17-10051-2017, 2017.
Rosen, J. M. and Kjome, N. T.: Backscattersonde: a new instrument for atmospheric aerosol research, Applied Optics, 30, 12, 1552-1561, 1991.
Sicard, M., D'Amico, G., Comerón Tejero, A., Mona, L., Alados Arboledas, L., Amodeo, A., Baars, H., Baldasano Recio, J. M., Belegante, L., Binietoglou, I., et al.: EARLINET: potential operationality of a research network, Atmospheric measurement techniques, 8, 4587–4613, 2015.
Vaisala: Vaisala Radiosonde RS41 Measurement Performance, White Paper, Vaisala, P.O. Box 26, Fl 00421, Helsinki, Finland, https://www.vaisala.com/sites/default/files/documents/WEA-MET-RS41-Performance-White-paper-B211356EN-B-LOW-v3.pdf, 2017 (accessed 8 January 2020).
Vernier, J.-P., Fairlie, T. D., Natarajan, M., Wienhold, F. G., Bian, J., Martinsson, B. G., Crumeyrolle, S., Thomason, L. W., and Bedka, K. M.: Increase in upper tropospheric and lower stratospheric aerosol levels and its potential connection with Asian pollution, J. Geophys. Res. Atmos., 120, 1608-1619, doi:10.1002/2014JD022372, 2015.
Vernier, J.-P., Fairlie, T. D., Deshler, T., Venkat Ratnam, M., Gadhavi, H., Kumar, B. S., Natarajan, M., Pandit, A. K., Akhil Raj, S. T., Hemanth Kumar, A., Jayaraman, A., Singh, A. K., Rastogi, N., Sinha, P. R., Kumar, S., Tiwari, S., Wegner, T., Baker, N., Vignelles, D., Stenchikov, G., Shevchenko, I., Smith, J., Bedka, K., Kesarkar, A., Singh, V., Bhate, J., Ravikiran, V., Durga Rao, M., Ravindrababu, S., Patel, A., Vernier, H., Wienhold, F. G., Liu, H., Knepp, T. N., Thomason, L., Crawford, J., Ziemba, L., Moore, J., Crumeyrolle, S., Williamson, M., Berthet, G., Jégou, F., and Renard, J.-B.: BATAL The Balloon Measurement Campaigns of the Asian Tropopause Aerosol Layer, Bull. Am. Meteorol. Soc., May 2018, 955-973, https://doi.org/10.1175/BAMS-D-17-0014.1, 2018.

Feldfunktion geändert

Watson-Parris, D., Schutgens, N., Reddington, C., Pringle, K. J., Liu, D., Allan, J. D., Coe, H., Carslaw, K. S., and Stier, P.: In situ constraints on the vertical distribution of global aerosol, Atmos. Chem. Phys., 19, 11765–11790, https://doi.org/10.5194/acp-19-11765-2019, 2019.

Weitkamp, C.: Lidar: Range-resolved Optical Remote Sensing of the Atmosphere, Springer Series in Optical Sciences, pp. 6-11, Ed. Springer, New York, USA, 2005.

Wandinger, U. and Ansmann, A.: Experimental determination of the lidar overlap profile with Raman lidar, Applied Optics, 41, 511-514, 2002.

Wiegner, M. and Geiss, A.: Aerosol profiling with the Jenoptik ceilometer CHM15kx, Atmos. Meas. Tech., 5, 1953–1964, https://doi.org/10.5194/amt-5-1953-2012, 2012.

Wendell, J., and Jordan, A.: iMet-1-RSB Radiosonde XDATA Protocol & Daisy Chaining, ftp://aftp.cmdl.noaa.gov/user/jordan/iMet-1-RSB Radiosonde XDATA Daisy Chaining.pdf , 2016 (accessed 3 March 2020).

Acknowledgements

This work has been supported by the Swiss National Science Foundation (project no. PZ00P2 168114 and project no. 200021_159950/2).

Data availability

The RALMO and CHM15K data can be accessed through the EARLINET (www.earlinet.org) and E-PROFILE (www.eumetnet.eu/e-profile) networks, respectively. The COBALD data can be obtained from the authors upon request.

Formatiert: Englisch (Vereinigte Staaten)

Formatiert: Absatz-Standardschriftart, Schriftart: 12 Pt., Englisch (Vereinigte Staaten)

Formatiert: Englisch (Vereinigte Staaten)

Formatiert: Englisch (Vereinigte Staaten)

Formatiert: Schriftart: Nicht Fett, Englisch (Vereinigte Staaten)

Formatiert: Englisch (Vereinigte Staaten)

Formatiert: Schriftart: Nicht Fett, Englisch (Vereinigte Staaten)

Formatiert: Englisch (Vereinigte Staaten)

Formatiert: Schriftart: Nicht Fett, Englisch (Vereinigte Staaten)

Technique	*Instrument*	*Type*	*Light source*	*Wavelenght(s)*	*Receiver FOV*
Remote sensing	RALMO	Raman lidar	Nd:YAG laser	355 nm	200 µrad (≈ 0.01°)
	CHM15K	Ceilometer (elastic backscatter lidar)	Nd:YAG laser	1064 nm	450 µrad (≈ 0.02°)
In-situ	COBALD	Balloon-borne backscatter sonde	LED	455, 940 nm	6°

Table 1. Summary of the main technical characteristics of the three instruments used in this work, including measuring technique, instrument type, light emitting source, wavelengths and receiver field of view (FOV) angle.

~~RALMO – COBALD (17 profiles, 2016-2019)~~

	~~Before FOV correction~~		~~After FOV correction~~	
~~*Interval*~~	~~*Mean $\Delta\beta_{aer}$ (455 nm)*~~	~~*Standard deviation*~~	~~*Mean $\Delta\beta_{aer}$ (455 nm)*~~	~~*Standard deviation*~~
~~0.8 < z < 2 km a.s.l.~~	~~+ 0.186 $Mm^{-1} sr^{-1}$ (+ 28.8 %)~~	~~± 0.300 $Mm^{-1} sr^{-1}$ (± 45.5 %)~~	~~+ 0.005 $Mm^{-1} sr^{-1}$ (+ 6.49 %)~~	~~± 0.319 $Mm^{-1} sr^{-1}$ (± 40.0 %)~~
~~2 < z < 4 km a.s.l.~~	~~+ 0.010 $Mm^{-1} sr^{-1}$ (+ 12.2 %)~~	~~± 0.101 $Mm^{-1} sr^{-1}$ (± 45.6 %)~~	~~− 0.008 $Mm^{-1} sr^{-1}$ (+ 6.60 %)~~	~~± 0.112 $Mm^{-1} sr^{-1}$ (± 43.3 %)~~
~~4 < z < 6 km a.s.l.~~	~~+ 0.025 $Mm^{-1} sr^{-1}$ (+ 33.4 %)~~	~~± 0.126 $Mm^{-1} sr^{-1}$ (± 95.2 %)~~	~~+ 0.021 $Mm^{-1} sr^{-1}$ (+ 28.6 %)~~	~~± 0.127 $Mm^{-1} sr^{-1}$ (± 95.0 %)~~
~~β_{aer} > 0.2 $Mm^{-1} sr^{-1}$~~	~~+ 0.173 $Mm^{-1} sr^{-1}$ (+ 25.9 %)~~	~~± 0.320 $Mm^{-1} sr^{-1}$ (± 61.4 %)~~	~~− 0.011 $Mm^{-1} sr^{-1}$ (+ 1.70 %)~~	~~± 0.329 $Mm^{-1} sr^{-1}$ (± 56.1 %)~~

RALMO – COBALD (17 profiles, 2016-2019, Medium-high aerosol content)

Altitude interval	*Mean deviation (δ)*	*Standard deviation (σ)*	*Correlation coefficient (ρ)*
0.8-3 km asl	− 0.018 $Mm^{-1} sr^{-1}$ (− 1.8 %)	0.237 $Mm^{-1} sr^{-1}$ (36.8 %)	+ 0.81
3- 6 km asl	+ 0.015 $Mm^{-1} sr^{-1}$ (+ 12.7 %)	0.068 $Mm^{-1} sr^{-1}$ (38.1 %)	+ 0.75
0.8- 6 km asl (i.e., all altitudes)	+ 0.001 $Mm^{-1} sr^{-1}$ (+ 6.4 %)	0.141 $Mm^{-1} sr^{-1}$ (37.6 %)	+ 0.80

Table 2. ~~Overview of the s~~Statistical comparison ~~of~~ of RALMO ~~vs~~vs. COBALD: results for medium-high aerosol content ~~(17 profiles, 2016-2019)~~. For each altitude interval~~For each data interval~~, we show mean ~~and standard deviation~~deviation (*δ*, both in absolute units and percent units relative to COBALD) and standard deviation (*σ*, both in absolute units and percent units relative to COBALD) at 455 nm, and ~~of the RALMO - COBALD difference in aerosol backscatter coefficient ($\Delta\beta_{aer}$) at 455 nm, calculated both before (left) and after (right) the FOV correction was applied to the COBALD data~~Pearson correlation coefficient (*ρ*). ~~Note that the data intervals are the same as those selected for the frequency of occurrence distributions shown in Figure 5 (2 km altitude bins between 0-6 km) and Figure 6 (all data points with COBALD β_{aer} > 0.2 $Mm^{-1} sr^{-1}$).~~

Formatiert: Englisch (Vereinigte Staaten)

Formatiert: Englisch (Vereinigte Staaten)

Formatiert: Englisch (Vereinigte Staaten)

Formatiert: Englisch (Vereinigte Staaten)

Formatiert: Schriftart: 11 Pt., Englisch (Vereinigte Staaten)

Formatiert: Zentriert

Formatierte Tabelle

Formatiert: Zentriert

Formatiert: Zentriert

Formatiert: Schriftart: Kursiv

Formatiert: Schriftart: Kursiv

~~CHM15K – COBALD (31 profiles, 2014-2019)~~

	~~Before FOV correction~~		~~After FOV correction~~	
~~*Interval*~~	~~*Mean* $\Delta\beta_{aer}$ *(940 nm)*~~	~~*Standard deviation*~~	~~*Mean* $\Delta\beta_{aer}$ *(940 nm)*~~	~~*Standard deviation*~~
~~0.8 < z < 2 km a.s.l.~~	~~+ 0.089 Mm⁻¹ sr⁻¹ (+ 25.2 %)~~	~~± 0.211 Mm⁻¹ sr⁻¹ (± 53.6 %)~~	~~+ 0.038 Mm⁻¹ sr⁻¹ (+ 13.1 %)~~	~~± 0.207 Mm⁻¹ sr⁻¹ (± 51.0 %)~~
~~2 < z < 4 km a.s.l.~~	~~+ 0.007 Mm⁻¹ sr⁻¹ (− 3.71 %)~~	~~± 0.150 Mm⁻¹ sr⁻¹ (± 322 %)~~	~~− 0.013 Mm⁻¹ sr⁻¹ (− 8.44 %)~~	~~± 0.162 Mm⁻¹ sr⁻¹ (± 320 %)~~
~~4 < z < 6 km a.s.l.~~	~~− 0.015 Mm⁻¹ sr⁻¹ (− 21.7 %)~~	~~± 0.119 Mm⁻¹ sr⁻¹ (± 644 %)~~	~~− 0.020 Mm⁻¹ sr⁻¹ (− 23.5 %)~~	~~± 0.139 Mm⁻¹ sr⁻¹ (± 641 %)~~
~~β_{aer} > 0.1 Mm⁻¹ sr⁻¹~~	~~+ 0.083 Mm⁻¹ sr⁻¹ (+ 16.2 %)~~	~~± 0.275 Mm⁻¹ sr⁻¹ (± 43.2 %)~~	~~− 0.001 Mm⁻¹ sr⁻¹ (+ 1.93 %)~~	~~± 0.281 Mm⁻¹ sr⁻¹ (± 42.5 %)~~

CHM15K – COBALD (31 profiles, 2014-2019, Medium-high aerosol content)

Altitude interval	*Mean deviation (δ)*	*Standard deviation (σ)*	*Correlation coefficient (ρ)*
0.8 – 3 km asl	+0.009 Mm^{-1} sr^{-1} (+ 5.2 %)	0.185 Mm^{-1} sr^{-1} (43.0 %)	+ 0.72
3 km – 6 km asl	− 0.081 Mm^{-1} sr^{-1} (− 43.3 %)	0.219 Mm^{-1} sr^{-1} (71.9 %)	+ 0.24
0.8- 6 km asl (i.e., all altitudes)	− 0.043 Mm^{-1} sr^{-1} (− 22.6 %)	0.205 Mm^{-1} sr^{-1} (59.6 %)	+ 0.62

Table 3. Statistical comparison of CHM15K vs. COBALD: results for medium-high aerosol content. For each altitude interval, we show mean deviation (*δ*, both in absolute units and percent units relative to COBALD) and standard deviation (*σ*, both in absolute units and percent units relative to COBALD) at 940 nm, and Pearson correlation coefficient (*ρ*).

~~**Table 3. Overview of the statistical comparison of CHM15K vs. COBALD (31 profiles, 2014-2019). For each data interval, we show mean and standard deviation (both in absolute units and percent units relative to COBALD) of the CHM15K - COBALD difference in aerosol backscatter coefficient ($\Delta\beta_{aer}$) at 940 nm, calculated both before (left) and after (right) the FOV correction was applied to the COBALD data. Note that the data intervals are the same as those selected for the frequency of occurrence distributions shown in Figure 8 (2 km altitude bins between 0-6 km) and Figure 9 (all data points with COBALD β_{aer} > 0.1 Mm⁻¹ sr⁻¹).**~~

Formatiert: Englisch (Vereinigte Staaten)

Formatiert: Englisch (Vereinigte Staaten)

Formatiert: Englisch (Vereinigte Staaten)

Formatiert: Englisch (Vereinigte Staaten)

Formatiert: Schriftart: 11 Pt., Englisch (Vereinigte Staaten)

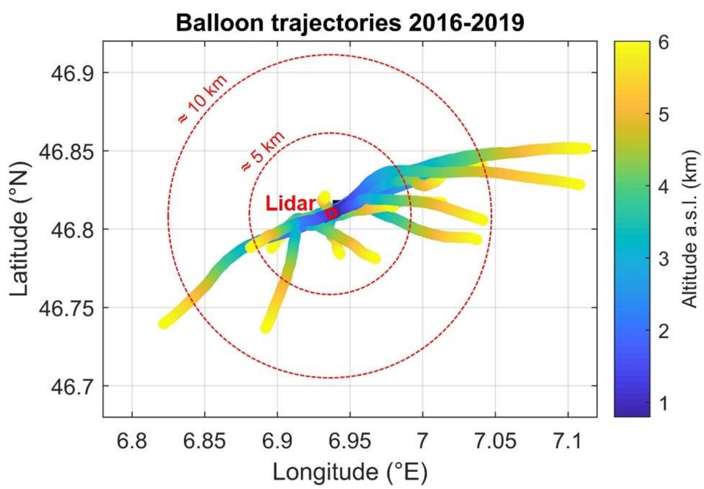

Figure 1. ~~Overview of b~~Balloon trajectories ~~as function of latitude,~~ (longitude vs. latitude) ~~and~~ as function of altitude (color scale)~~,~~ for all the analyzed soundings of the RALMO vs. COBALD comparison ~~in the period~~(~~-~~17 profiles, 2016-2019~~ (total 17 profiles, corresponding to the dataset used for the RALMO vs. COBALD comparison~~). The ~~balloon~~ trajectories are ~~color-coded with altitude and~~ plotted with vertical resolution of 30 m between ~~800~~ 0.8~~m~~ - 6 km altitude asl. The location of the RALMO and CHM15K lidars (and balloon launching site) is shown by the solid red circle (46.82°E, 6.95°N). Two dotted red circles indicate horizontal distances of approximately 5 km and 10 km from the lidar site.

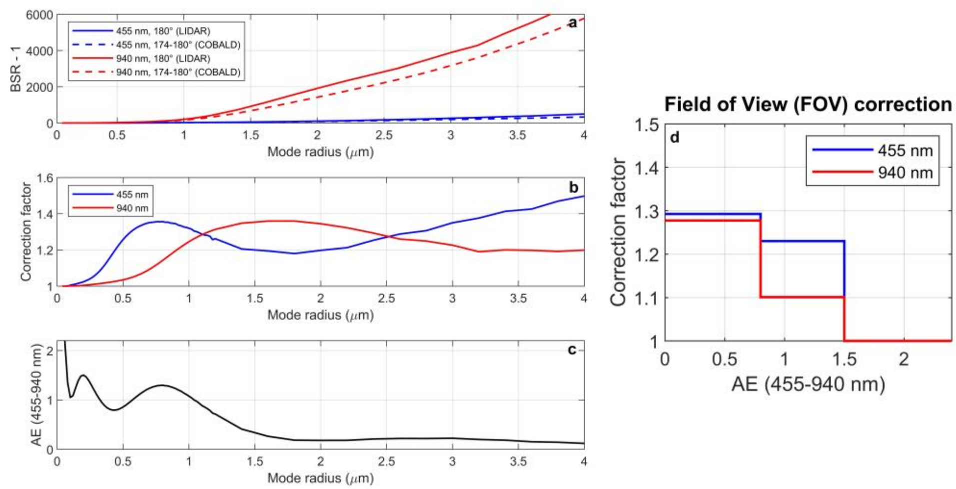

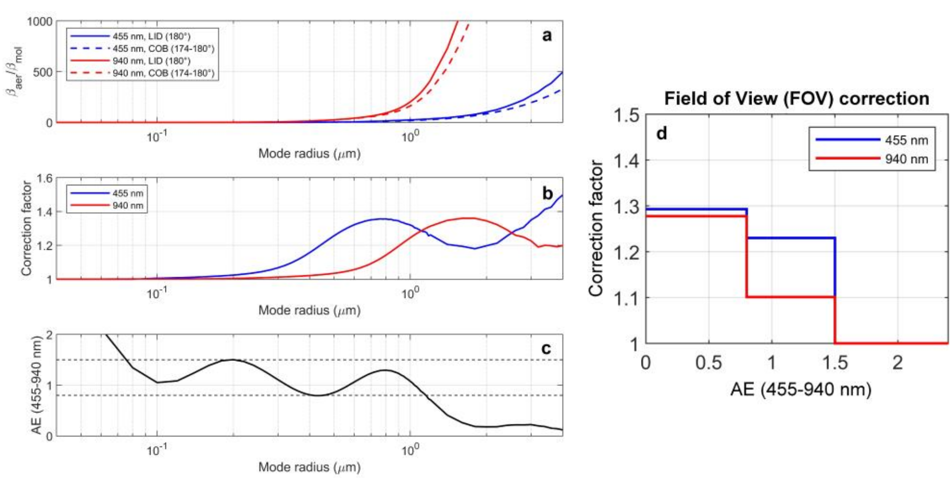

Figure 2. Mie-theory scattering model simulations. Panel (a): ratio of ~~a~~aerosol-to-molecular backscatter coefficient, β_{aer}/β_{mol} (i.e., BSR − 1) at 455 nm (blue) and 940 nm (red), ~~backscatter ratio (BSR) − 1~~ as function of mode radius (R_m), calculated assuming a field of

Formatiert: Schriftart: 9 Pt., Fett

view (FOV) angle of 174°-180° (dashed lines, COBALD) and 180° (solid lines, lidar), and aerosol number concentration $N = 10^3$ cm^{-3}. Panel (b): correction factors, i.e. lidar-to-COBALD ratio of β_{aer}/β_{mol} ~~BSR − 1~~ (as shown in Panel a) for 455 nm (blue) and 940 nm (red), as function of R_m. Panel (c): simulated Angstrom exponent (AE) for the COBALD wavelength interval (455-940 nm), as function of R_m. Black dashed lines indicate the thresholds of AE = 0.8 and AE = 1.5 used for the parameterization of the correction factors (see Section 3.2). Panel (d): resulting FOV correction as function of AE.

Formatiert: Schriftart: Kursiv

Formatiert: Schriftart: 9 Pt., Fett

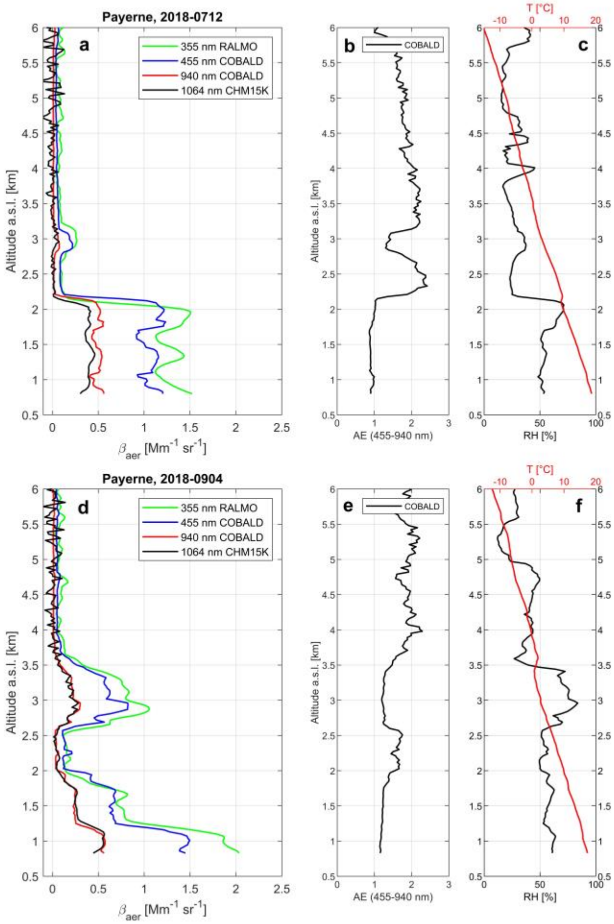

Figure 3. Overview of selected profiles measured on 7 July 2018 (Panels a-c) and 4 September 2018 (Panels d-f). Panels (a, c): vertical profiles of aerosol backscatter coefficient (β_{aer}) as function of altitude, measured by RALMO (355 nm, green), COBALD (455 nm, blue and 940 nm, red) and CHM15K (1064 nm, black). Panels (b, d): vertical profiles of Angstrom exponent (AE) for wavelengths 455-940 nm, calculated from the COBALD data. Panels (c, f): vertical profiles of relative humidity (RH, black) and temperature (red, top scale) measured by the Vaisala RS41-SGP radiosonde (flying in tandem with the COBALD sonde).

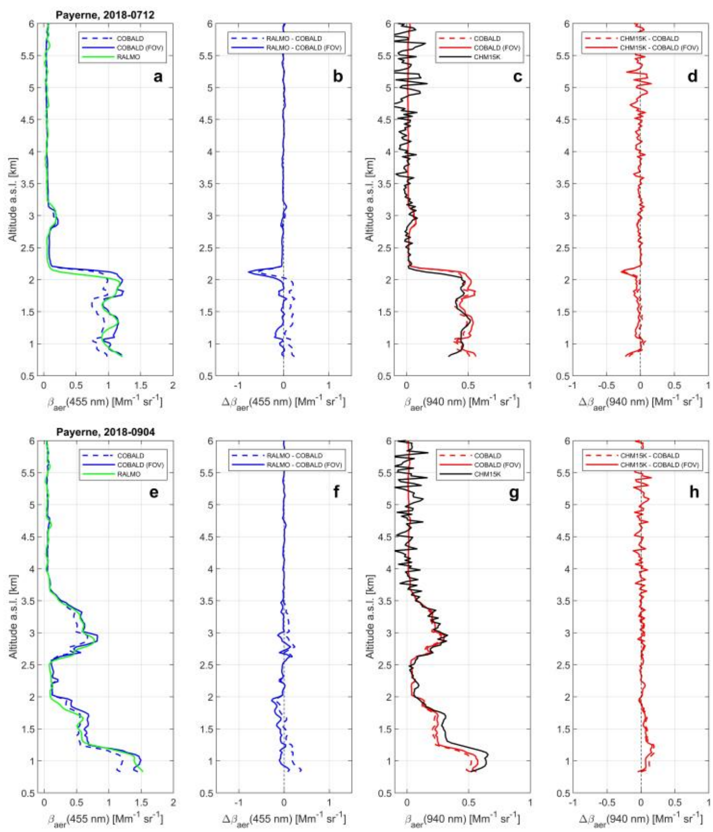

Figure 4. Quantitative comparison of RALMO vs. COBALD (Panels a-b, e-f) and CHM15K vs. COBALD (Panels c-d, g-h) for the selected profiles measured on 7 July 2018 (Panels a-d) and 4 September 2018 (Panels e-h). Panels (a, e): vertical profiles of aerosol backscatter coefficient (β_{aer}) at 455 nm measured by RALMO (green) and COBALD (blue), both without (dashed) and with (solid) application of the FOV correction. Panels (b, f): vertical profiles of the RALMO – COBALD difference in β_{aer} ($\Delta\beta_{aer}$) at 455 nm, both without (dashed) and with (solid) application of the FOV correction. Panels (c, g): vertical profiles of β_{aer} at 940 nm measured by CHM15K (black) and COBALD (red), both without (dashed) and with (solid) FOV correction. Panels (d, h): vertical profiles of $\Delta\beta_{aer}$ for CHM15k – COBALD at 940 nm, both without (dashed) and with (solid) FOV correction.

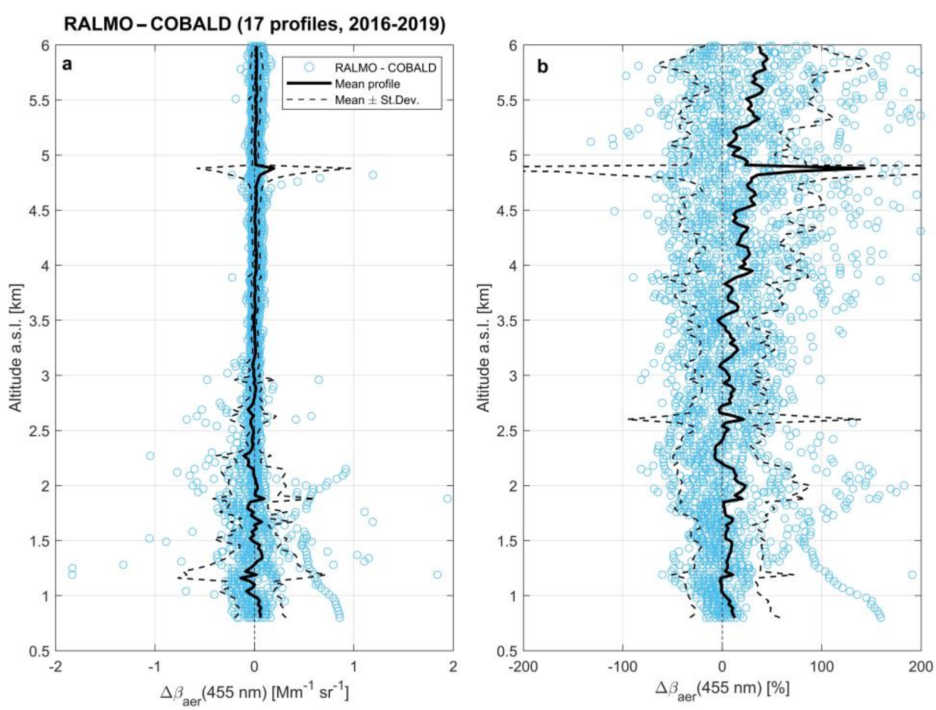

Formatiert: Einzug: Links: -1.3 cm

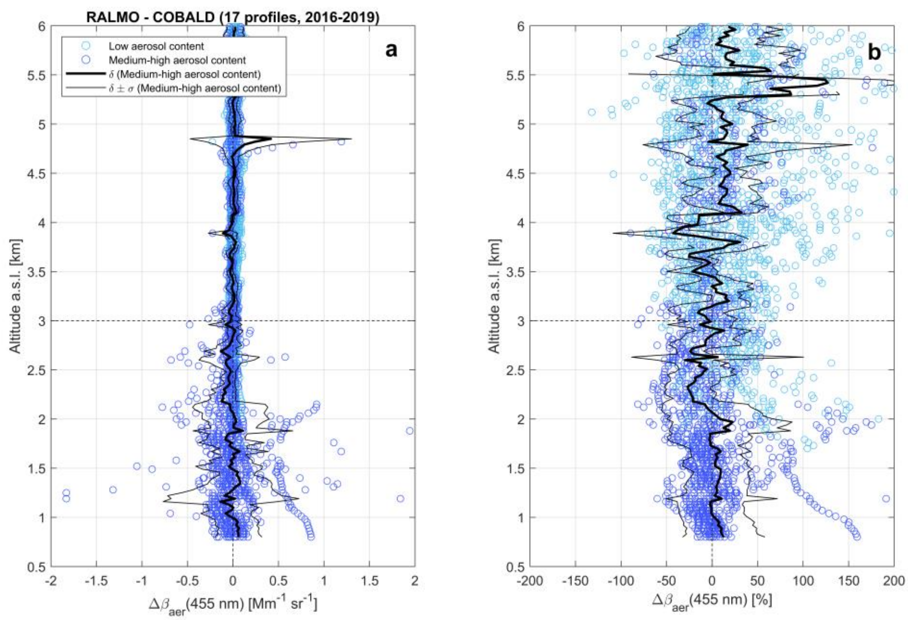

Figure 5. Statistical comparison of RALMO vs. COBALD~~ (17 profiles, 2016-2019)~~: vertical profiles. Panel (a): all ~~data points~~medium-high aerosol content (dark blue circles)~~,~~ and ~~mean profile~~Low aerosol content (~~thick solid black line~~light blue circles) ~~and mean ± standard deviation profiles (thin dashed black lines)~~ data points of the RALMO – COBALD ~~difference in~~ aerosol backscatter coefficient difference ($\Delta\beta_{aer}$) at 455 nm, as function of altitude. Panel (b): same as Panel (a), with $\Delta\beta_{aer}$ expressed in percent units (%) relative to the COBALD measurements~~ (instead of absolute backscatter coefficient units, Mm^{-1} sr^{-1})~~. Mean deviation (δ) and mean ± standard deviation ($\delta \pm \sigma$) profiles are shown in both panels by thick solid and thin dashed black lines, respectively. The 3 km altitude level is highlighted by a thin dashed black line.

Formatiert: Schriftart: 9 Pt., Fett

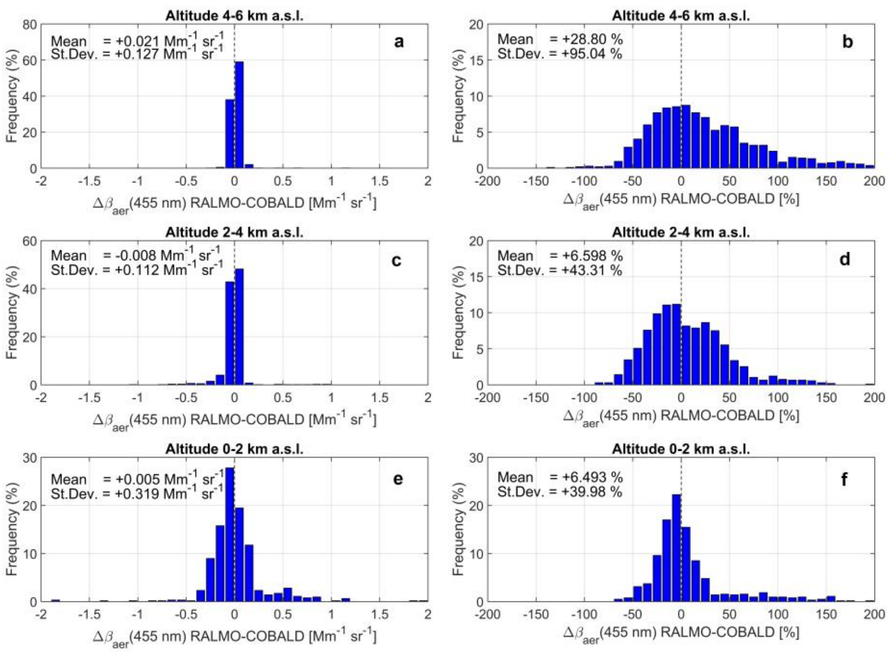

Altitude 4-6 km a.s.l.
Mean = +0.021 Mm-1 sr-1
St.Dev. = +0.127 Mm-1 sr-1
a
Frequency (%)
Δβaer(455 nm) RALMO-COBALD [Mm-1 sr-1]
Altitude 4-6 km a.s.l.
Mean = +28.80 %
St.Dev. = +95.04 %
b
Δβaer(455 nm) RALMO-COBALD [%]
Altitude 2-4 km a.s.l.
Mean = -0.008 Mm-1 sr-1
St.Dev. = +0.112 Mm-1 sr-1
c
Altitude 2-4 km a.s.l.
Mean = +6.598 %
St.Dev. = +43.31 %
d
Altitude 0-2 km a.s.l.
Mean = +0.005 Mm-1 sr-1
St.Dev. = +0.319 Mm-1 sr-1
e
Altitude 0-2 km a.s.l.
Mean = +6.493 %
St.Dev. = +39.98 %
f

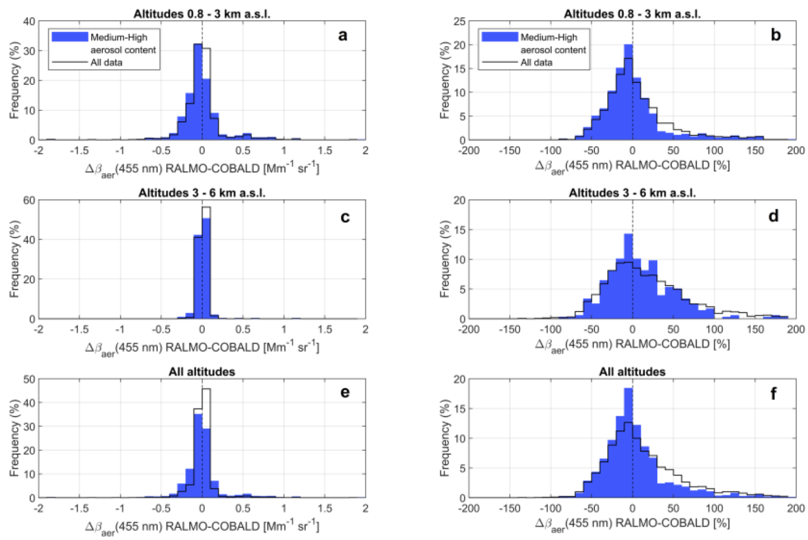

Figure 6. Statistical comparison of RALMO vs. COBALD: ~~(17 profiles, 2016-2019):~~ frequency of occurrence distributions of medium-high aerosol content data (blue bars) and all data (black lines). Panels (~~(~~a, c, e~~)~~): frequency of occurrence distributions of the RALMO – COBALD difference in aerosol backscatter coefficient ($\Delta\beta_{aer}$) at 455 nm, for the altitude intervals ~~0-2~~0.8-3 km asl (Panel ~~Panel e~~a), ~~2~~3-~~4~~6 km (Panel ~~e~~c) and ~~4-6~~0.8-6 km ~~km~~ asl (i.e., all altitudes: Panel e~~a~~). ~~above sea level (a.s.l.).~~ Panels (~~(~~b, d, f): same as Panels (~~(~~a, c, e)~~)~~, with $\Delta\beta_{aer}$ expressed in percent units (%) relative to the COBALD measurements (instead of absolute backscatter coefficient units, Mm^{-1} sr^{-1}). ~~Mean value and standard deviation of the distributions are displayed in each panel.~~ The frequency of occurrence distributions are calculated in $\Delta\beta_{aer}$ intervals of 0.1 Mm^{-1} sr^{-1} (Panels a, c, e) and 10% (Panels a, c, e).

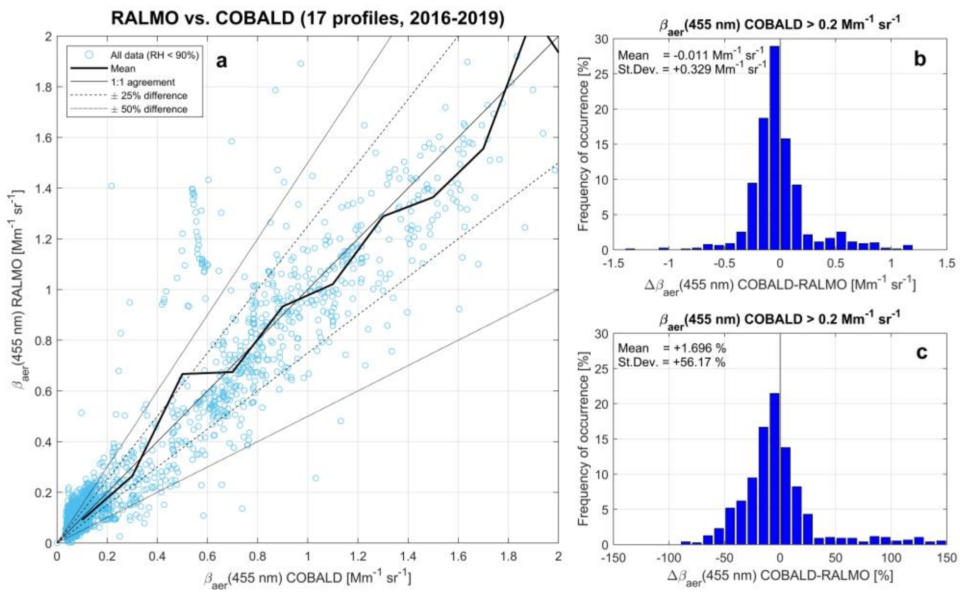

RALMO vs. COBALD (17 profiles, 2016-2019)
All data (RH < 90%)
Mean
1:1 agreement
± 25% difference
± 50% difference
a
β_{aer}(455 nm) RALMO [Mm^{-1} sr^{-1}]
β_{aer}(455 nm) COBALD [Mm^{-1} sr^{-1}]
β_{aer}(455 nm) COBALD > 0.2 Mm^{-1} sr^{-1}
Mean = -0.011 Mm^{-1} sr^{-1}
St.Dev. = +0.329 Mm^{-1} sr^{-1}
b
Frequency of occurrence [%]
$\Delta\beta_{aer}$(455 nm) COBALD-RALMO [Mm^{-1} sr^{-1}]
β_{aer}(455 nm) COBALD > 0.2 Mm^{-1} sr^{-1}
Mean = +1.696 %
St.Dev. = +56.17 %
c
Frequency of occurrence [%]
$\Delta\beta_{aer}$(455 nm) COBALD-RALMO [%]

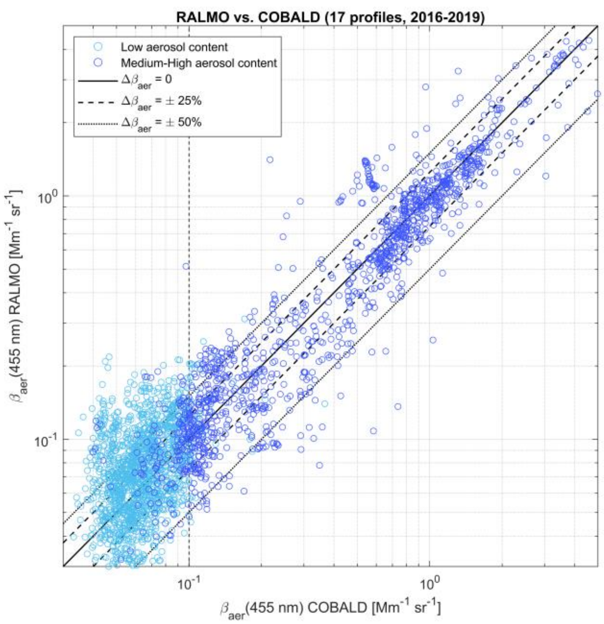

Figure 7. Statistical comparison of RALMO vs. COBALD ~~(17 profiles, 2016-2019)~~: scatter plot ~~and frequency of occurrence distributions. Panel (a): scatter plot~~. All ~~of~~ medium-high aerosol content (dark blue circles) and Low aerosol content (light blue circles) data points of ~~all data points (blue circles) of~~ aerosol backscatter coefficient (β_{aer}) at 455 nm measured by RALMO (y-axis) vs. β_{aer} at 455 nm measured by COBALD (x-axis). Thin black lines ~~identify the~~show 1:1 agreement (solid), ~~isoline between RALMO and COBALD (solid),~~ ±25 % differences (dashed) and ±50 % differences (dotted) isolines. The 0.1 Mm^{-1} sr^{-1} threshold in COBALD β_{aer}, separating low from medium-high aerosol content data at 455 nm (as described in Section 3.3), is shown by a vertical black dashed line.

~~The thick solid black lines shows the mean β_{aer} from RALMO calculated for each 0.2 Mm^{-1} sr^{-1} interval of β_{aer} from COBALD. Panels (b-c): frequency of occurrence distributions of RALMO – COBALD difference in β_{aer} ($\Delta\beta_{aer}$), calculated for all data points with COBALD β_{aer}^{455} > 0.2 Mm^{-1} sr^{-1} at 455 nm.~~

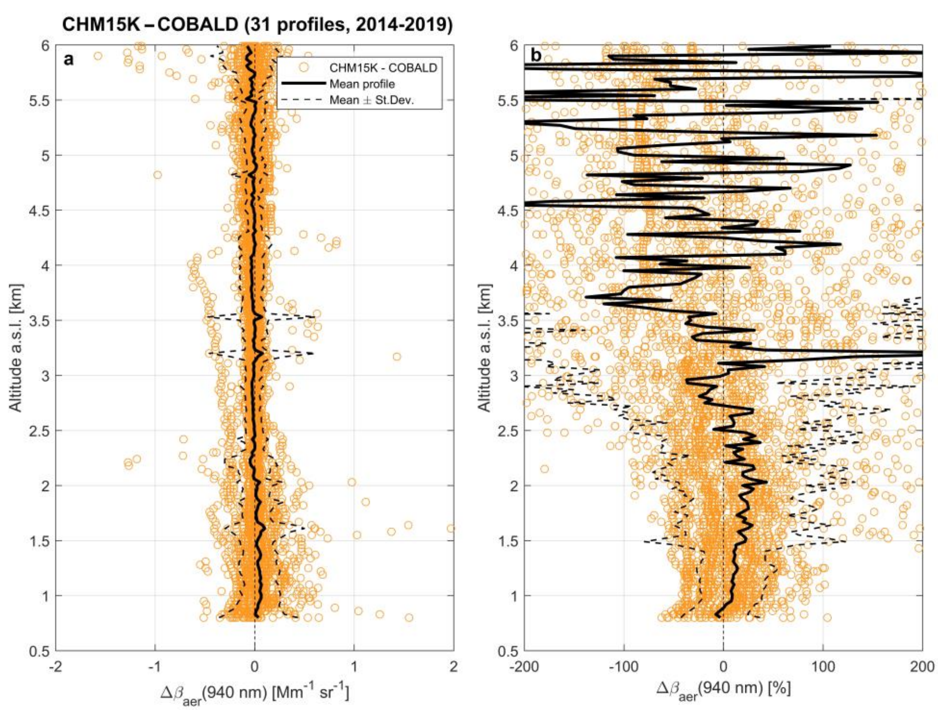

Formatiert: Einzug: Links: -1.3 cm

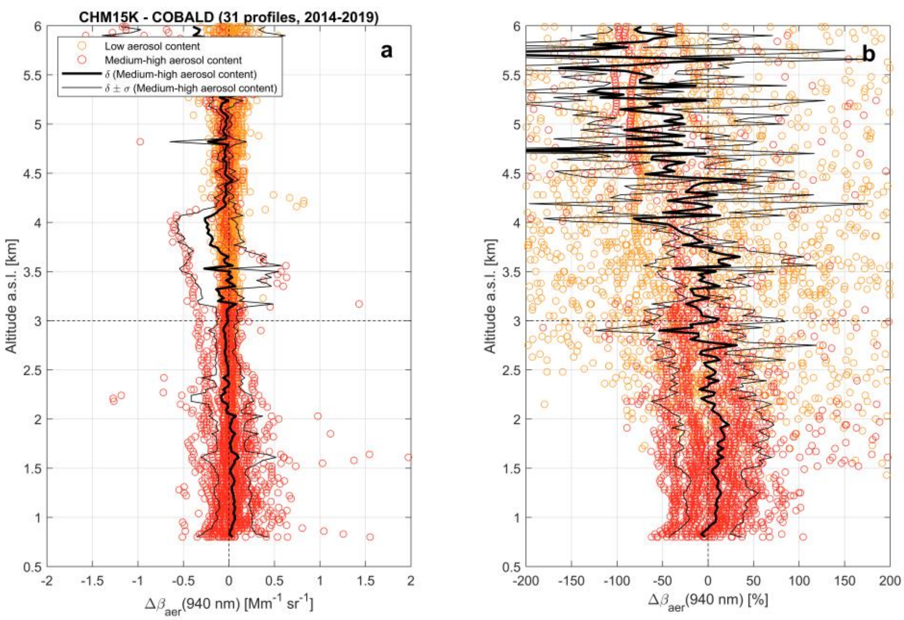

Figure 8. Statistical comparison of CHM15K vs. COBALD: vertical profiles. Panel (a): all Medium-high aerosol content (red circles) and Low aerosol content (orange circles) data points of CHM15K – COBALD aerosol backscatter coefficient difference (*Δβ*$_{aer}$) at 940 nm, as function of altitude. Panel (b): same as Panel (a), with *Δβ*$_{aer}$ expressed in percent units (%) relative to the COBALD measurements. Mean deviation (*δ*) and mean ± standard deviation (*δ* ± *σ*) profiles are shown in both panels by thick solid and thin dashed black lines, respectively. The 3 km altitude level is highlighted by a thin dashed black line.

~~Statistical comparison of CHM15K vs. COBALD (31 profiles, 2014-2019): vertical profiles. Panel (a): all data points (blue circles), mean profile (thick solid black line) and mean ± standard deviation profiles (thin dashed black lines) of CHM15K – COBALD difference in aerosol backscatter coefficient (Δβaer) at 940 nm, as function of altitude. Panel (b): same as Panel (a), with Δβaer expressed in percent units (%) relative to the COBALD measurements (instead of absolute backscatter coefficient units, Mm-1 sr-1).~~

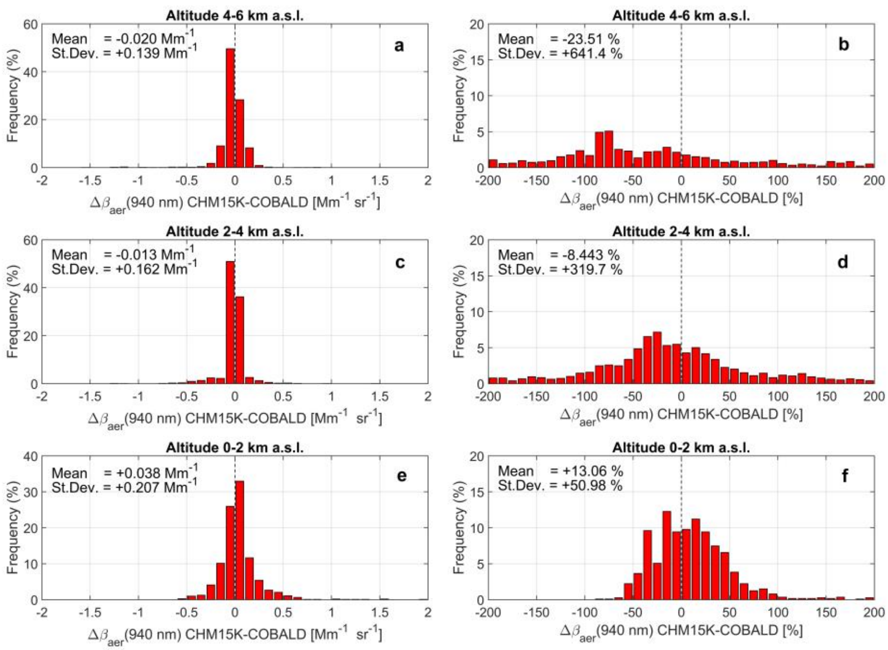

Altitude 4-6 km a.s.l.
Mean = -0.020 Mm-1
St.Dev. = +0.139 Mm-1
a
Frequency (%)
Δβaer(940 nm) CHM15K-COBALD [Mm-1 sr-1]
Altitude 4-6 km a.s.l.
Mean = -23.51 %
St.Dev. = +641.4 %
b
Δβaer(940 nm) CHM15K-COBALD [%]
Altitude 2-4 km a.s.l.
Mean = -0.013 Mm-1
St.Dev. = +0.162 Mm-1
c
Altitude 2-4 km a.s.l.
Mean = -8.443 %
St.Dev. = +319.7 %
d
Altitude 0-2 km a.s.l.
Mean = +0.038 Mm-1
St.Dev. = +0.207 Mm-1
e
Altitude 0-2 km a.s.l.
Mean = +13.06 %
St.Dev. = +50.98 %
f

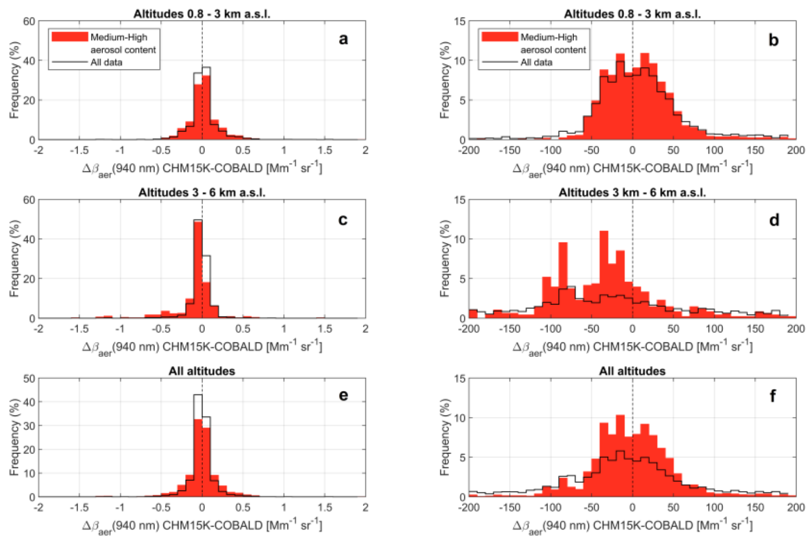

Figure 9. Statistical comparison of CHM15K vs. COBALD: frequency of occurrence distributions of medium-high aerosol content data (blue bars) and all data (black lines). Panels (a, c, e): frequency of occurrence distributions of the CHM15K – COBALD difference in aerosol backscatter coefficient (*$\Delta\beta_{aer}$*) at 940 nm, for the altitude intervals 0.8-3 km asl (Panel a), 3-6 km (Panel c) and 0.8-6 km asl (i.e., all altitudes: Panel e). Panels (b, d, f): same as Panels (a, c, e), with *$\Delta\beta_{aer}$* expressed in percent units (%) relative to the COBALD measurements (instead of absolute backscatter coefficient units, Mm^{-1} sr^{-1}). The frequency of occurrence distributions are calculated in *$\Delta\beta_{aer}$* intervals of 0.1 Mm^{-1} sr^{-1} (Panels a, c, e) and 10% (Panels a, c, e).

~~Figure 9. Statistical comparison of CHM15K vs. COBALD (31 profiles, 2014-2019): frequency of occurrence distributions. Panels (a, c, e): frequency of occurrence distributions of CHM15K – COBALD difference in aerosol backscatter coefficient ($\Delta\beta_{aer}$) at 940 nm, for the altitude intervals 0-2 km (Panel e), 2-4 km (c) and 4-6 km (a) above sea level (a.s.l.). Panels (b, d, f): same as Panels (a, c, e), with $\Delta\beta_{aer}$ expressed in percent units (%) relative to the COBALD measurements (instead of absolute backscatter coefficient units, Mm^{-1} sr^{-1}). Mean value and standard deviation of the distributions are displayed in each panel. The frequency of occurrence distributions are calculated in $\Delta\beta_{aer}$ intervals of 0.1 Mm^{-1} sr^{-1} (Panels a, c, e) and 10% (Panels a, c, e).~~

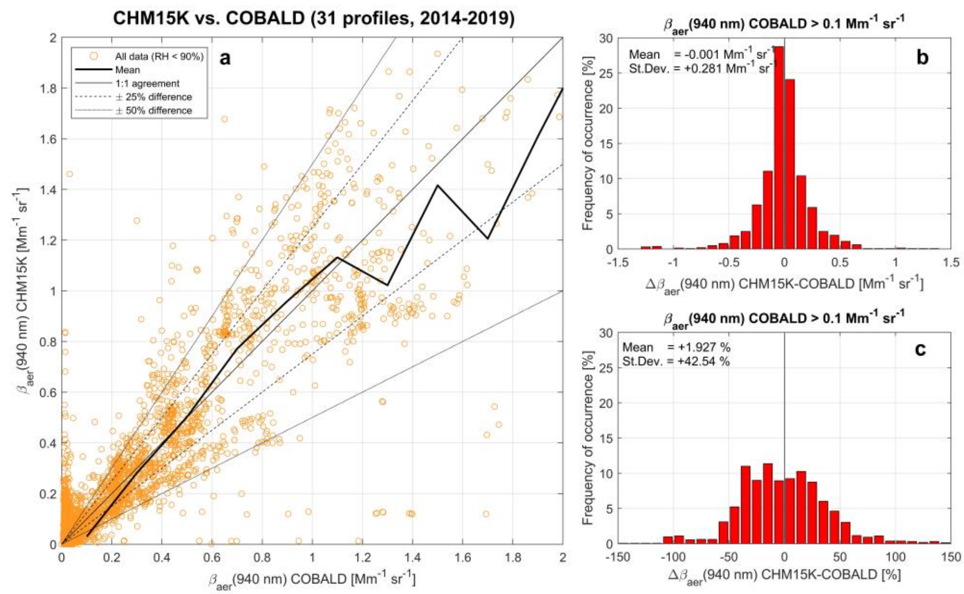
CHM15K vs. COBALD (31 profiles, 2014-2019)
All data (RH < 90%)
Mean
1:1 agreement
± 25% difference
± 50% difference
a
β_{aer}(940 nm) CHM15K [Mm^{-1} sr^{-1}]
β_{aer}(940 nm) COBALD [Mm^{-1} sr^{-1}]
β_{aer}(940 nm) COBALD > 0.1 Mm^{-1} sr^{-1}
Mean = -0.001 Mm^{-1} sr^{-1}
St.Dev. = +0.281 Mm^{-1} sr^{-1}
b
Frequency of occurrence [%]
$\Delta\beta_{aer}$(940 nm) CHM15K-COBALD [Mm^{-1} sr^{-1}]
β_{aer}(940 nm) COBALD > 0.1 Mm^{-1} sr^{-1}
Mean = +1.927 %
St.Dev. = +42.54 %
c
Frequency of occurrence [%]
$\Delta\beta_{aer}$(940 nm) CHM15K-COBALD [%]

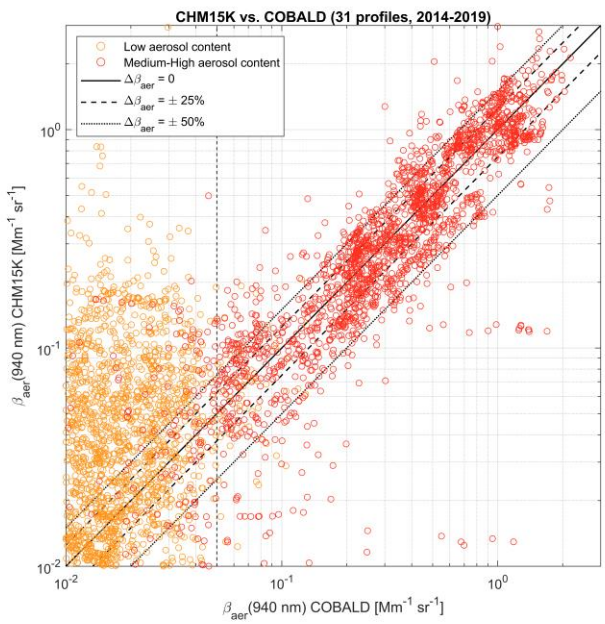

Figure 10. Statistical comparison of CHM15K vs. COBALD: scatter plot. All Medium-high aerosol content (red circles) and Low aerosol content (orange circles) data points of aerosol backscatter coefficient (*β_{aer}*) at 940 nm measured by CHM15K (y-axis) vs. *β_{aer}* at 940 nm measured by COBALD (x-axis). Thin black lines show 1:1 agreement (solid), ±25 % differences (dashed) and ±50 % differences (dotted) isolines. The 0.05 Mm^{-1} sr^{-1} threshold in COBALD *β_{aer}*, separating Low from Medium-high aerosol content data at 940 nm (as described in Section 3.3), is shown by a vertical black dashed line.

~~**Figure 10. Statistical comparison of CHM15K vs. COBALD (31 profiles, 2014-2019): scatter plot and frequency of occurrence distributions. Panel (a): scatter plot of all data points (blue circles) of aerosol backscatter coefficient (β_{aer}) at 940 nm measured by CHM15K (y-axis) vs. β_{aer} at 455 nm measured by COBALD (x-axis). Thin black lines identify the 1:1 agreement isoline between CHM15K and COBALD (solid), ±25 % differences (dashed) and ±50 % differences (dotted). The thick solid black lines shows the mean β_{aer} from CHM15K calculated for each 0.2 Mm^{-1} sr^{-1} interval of β_{aer} from COBALD. Panels (b-c): frequency of occurrence distributions of CHM15K – COBALD difference in β_{aer} ($\Delta\beta_{aer}$), calculated for all data points with COBALD β_{aer}^{940} > 0.1 Mm^{-1} sr^{-1} at 940 nm.**~~